

Chapter 15

AC Motor Speed Control

T.A. Lipo

University of Wisconsin
Madison WI, U.S.A

Karel Jezernik

University of Maribor
Maribor Slovenia

15.1 Introduction

An important factor in industrial progress during the past five decades has been the increasing sophistication of factory automation which has improved productivity manyfold. Manufacturing lines typically involve a variety of variable speed motor drives which serve to power conveyor belts, robot arms, overhead cranes, steel process lines, paper mills, and plastic and fiber processing lines to name only a few. Prior to the 1950s all such applications required the use of a DC motor drive since AC motors were not capable of smoothly varying speed since they inherently operated synchronously or nearly synchronously with the frequency of electrical input. To a large extent, these applications are now serviced by what can be called general-purpose AC drives. In general, such AC drives often feature a cost advantage over their DC counterparts and, in addition, offer lower maintenance, smaller motor size, and improved reliability. However, the control flexibility available with these drives is limited and their application is, in the main, restricted to fan, pump, and compressor types of applications where the speed need be regulated only roughly and where transient response and low-speed performance are not critical.

More demanding drives used in machine tools, spindles, high-speed elevators, dynamometers, mine winders, rolling mills, glass float lines, and the like have much more sophisticated requirements and must afford the flexibility to allow for regulation of a number of variables, such as speed, position, acceleration, and torque. Such high-performance applications typically require a high-speed holding accuracy better than 0.25%, a wide speed range of at least 20:1, and fast transient response, typically better than 50 rad/s, for the speed loop. Until recently, such drives were almost exclusively the domain of DC motors combined with various configurations of AC-to-DC converters depending upon the application. With suitable control, however, induction motor drives

have been shown to be more than a match for DC drives in high-performance applications. While control of the induction machine is considerably more complicated than its DC motor counterpart, with continual advancement of microelectronics, these control complexities have essentially been overcome. Although induction motor drives have already overtaken DC drives during the next decade it is still too early to determine if DC drives will eventually be relegated to the history book. However, the future decade will surely witness a continued increase in the use of AC motor drives for all variable speed applications.

AC motor drives can be broadly categorized into two types, thyristor based and transistor based drives. Thyristors possess the capability of self turn-on by means of an associated gate signal but must rely upon circuit conditions to turn off whereas transistor devices are capable of both turn-on and turn-off. Because of their turn-off limitations, thyristor based drives must utilize an alternating EMF to provide switching of the devices (commutation) which requires reactive volt-amperes from the EMF source to accomplish.

A brief list of the available drive types is given in Figure 15.1. The drives are categorized according to switching nature (natural or force commutated), converter type and motor type. Naturally commutated devices require external voltage across the power terminals (anode-cathode) to accomplish turn-off of the switch whereas a force commutated device uses a low power gate or base voltage signal which initiates a turn-off mechanism in the switch itself. In this figure the category of transistor based drives is intended to also include other hard switched turn-off devices such as GTOs, MCTs and IGCTs which are, in reality, avalanche turn-on (four-layer) devices.

The numerous drive types associated with each category is clearly extensive and cannot be treated in complete detail here. However, the speed control of the four major drive types having differing control principles will be considered namely 1) voltage controlled induction motor drives 2) load commutated synchronous motor drives, 3) volts per hertz and vector controlled induction motor drives and 4) vector controlled permanent magnet motor drives. The control principles of the remaining drives of Figure 15.1 are generally straightforward variations of one of these four drive types.

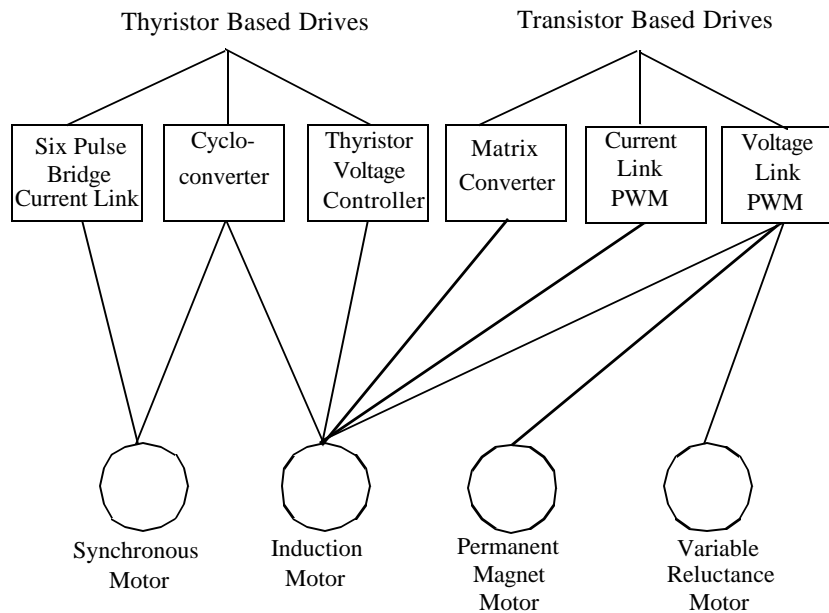


Figure 15.1 Major drive type categories

15.2 Thyristor Based Voltage Controlled Drives

15.2.1 Introduction

During the middle of the last century, limitations in solid state switch technology hindered the performance of variable frequency drives. In what was essentially a stop-gap measure, variable speed was frequently obtained by simply varying the voltage to an induction motor while keeping the frequency constant. The switching elements used were generally back-to-back connected thyristors as shown in Figure 15.2. These devices were exceptionally rugged compared to the fragile transistor devices of this era.

15.2.2 Basic Principles of Voltage Control

The basic principles of voltage control can be obtained readily from the conventional induction motor equivalent circuit shown in Figure 15.3 and the

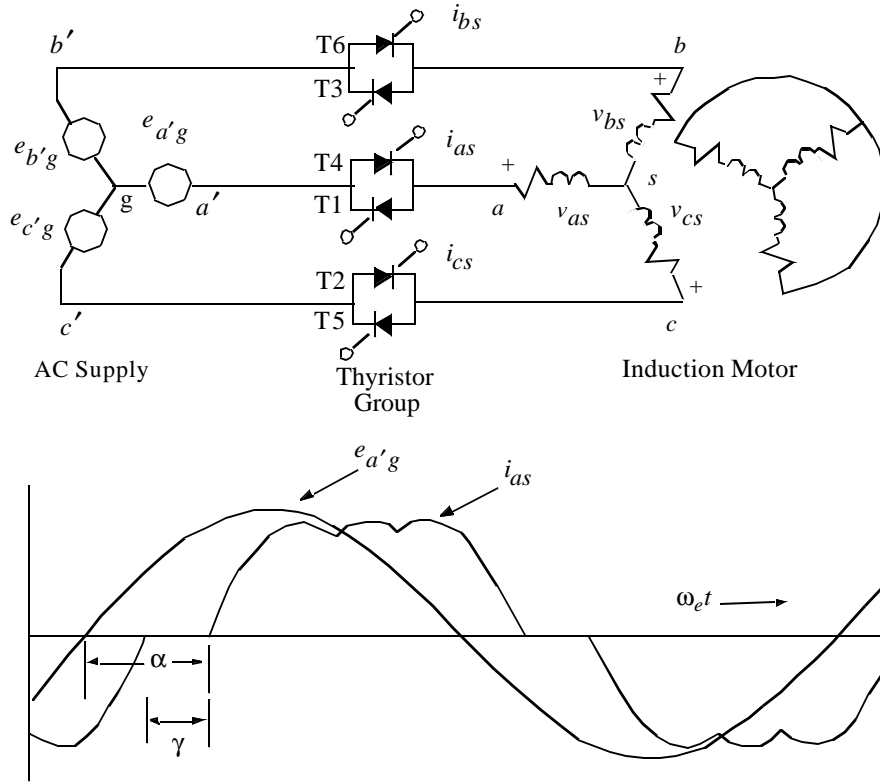


Figure 15.2 Induction motor voltage controller employing inverse-parallel thyristors and typical current waveform

associated constant voltage speed-torque curves illustrated in Figure 15.4. The torque produced by the machine is equal to the power transferred across the airgap divided by synchronous speed,

$$T_e = \frac{3}{2} P \left(\frac{I_2^2 r_2}{S \omega_e} \right) \quad (15.1)$$

where P = number of poles, S is the per unit slip, ω_e is line frequency and I_2 , r_2 are the rotor rms current and rotor resistance respectively.

The peak torque points on the curves in Figure 15.4 occur when maximum power is transferred across the airgap and are easily shown to take place at a slip,

$$S_{MaxT} \approx \frac{r_2}{x_1 + x_2} \quad (15.2)$$

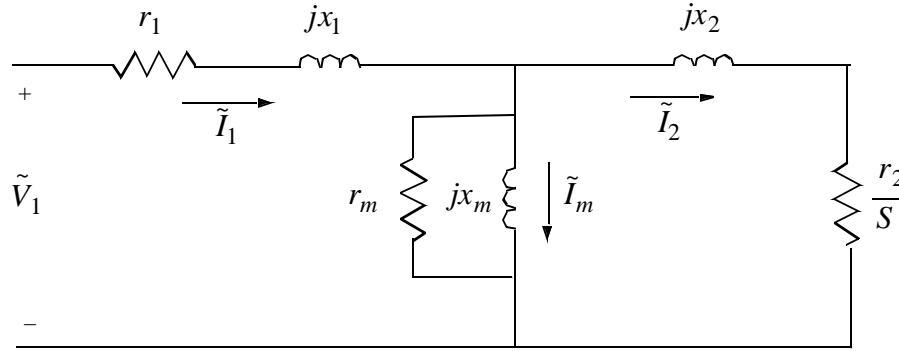


Figure 15.3 Per phase equivalent circuit of a squirrel cage induction machine

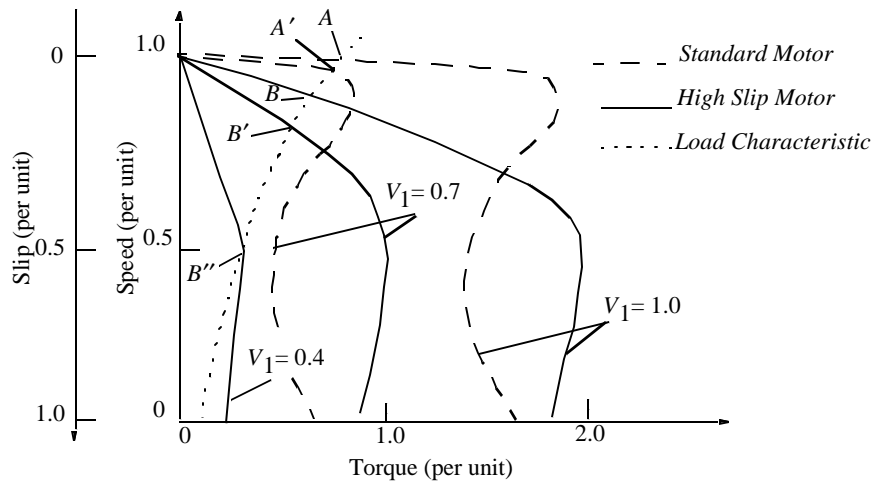


Figure 15.4 Torque versus speed curves for standard and high slip induction machines

where x_1 and x_2 are the stator and rotor leakage reactances. From these results and the equivalent circuit, the following principles of voltage control are evident:

- (1) For any fixed slip or speed, the current varies directly with voltage and the torque and power with voltage squared.
- (2) As a result of (1) the torque-speed curve for a reduced voltage maintains its shape exactly but has reduced torque at all speeds, see Figure 15.4.
- (3) For a given load characteristic, a reduction in voltage will produce an increase in slip (from A to A' for the conventional machine in Figure 15.4, for example).

(4) A high-slip machine has relatively higher rotor resistance and results in a larger speed change for a given voltage reduction and load characteristic (compare A to A' with B to B' in Figure 15.4).

(5) At small values of torque, the slip is small and the major power loss is the core loss in r_m . Reducing the voltage will reduce the core loss at the expense of higher slip and increased rotor and stator $I^2 r$ loss. Thus there is an optimal slip which maximizes the efficiency and varying the voltage can maintain high efficiency even at low torque loads.

15.2.3 Converter Model of Voltage Controller

It has been shown that a very accurate fundamental component model for a voltage converter comprised of inverse parallel thyristors (or Triacs) is a series reactance given by [1]:

$$x_{eq} = x_s' f(\gamma) \quad (15.3)$$

where $x_s' = x_1 + x_2 x_m / (x_2 + x_m)$ and x_1, x_2, x_m are the induction motor stator leakage, rotor leakage and magnetizing reactances respectively and γ is the thyristor *hold-off angle* identified in Figure 15.2 and

$$f(\gamma) = \left(\frac{3}{\pi}\right) \frac{(\gamma + \sin\gamma)}{1 - \frac{3}{\pi}(\gamma + \sin\gamma)} \quad (15.4)$$

This reactance can be added in series with the motor equivalent circuit to model a voltage-controlled system. For typical machines the accuracy is well within acceptable limits although the approximation is better in larger machines and for smaller values of γ . In most cases of interest, the error is quite small. However, the harmonic power losses and torque ripple produced by the current harmonics implied in Figure 15.2 are entirely neglected. A plot of typical torque versus speed characteristics as a function of γ is shown in Figure 15.5 for a 0.4 hp squirrel cage induction machine [2].

15.2.4 Speed Control of Voltage Controlled Drive

Variable-voltage speed controllers must contend with the problem of greatly increased slip losses at speeds far from synchronous and the resulting low efficiency. In addition, only speeds below synchronous speed are attainable and speed stability may be a problem unless some form of feedback is employed.

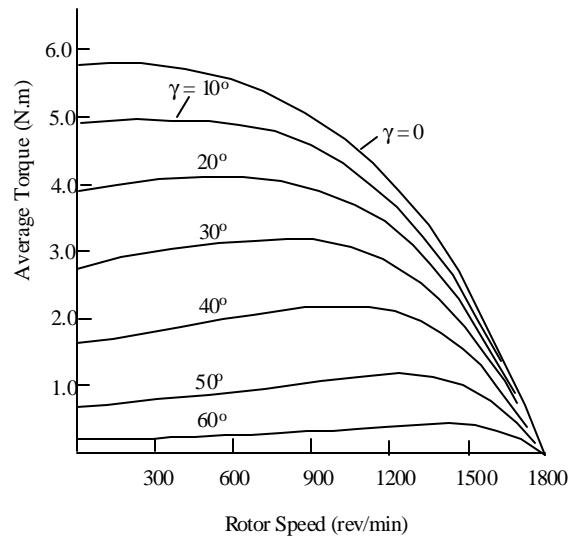


Figure 15.5 Torque speed curves for changes in hold off angle γ

An appreciation of the efficiency and motor heating problem is available from Equation (15.1) rewritten to focus on the rotor $I_2^2 r$ loss,

$$3I_2^2 r_2 = SP_{gap} = S \frac{2}{P} \omega_e T_e \quad (15.5)$$

Thus the rotor copper loss is proportional not only to the torque but also to the slip (deviation from synchronous speed). The inherent problem of slip variation for speed control is clearly indicated.

As a result of the large rotor losses to be expected at high slip, voltage control is only applicable to loads in which the torque drops off rapidly as the speed is reduced. The most important practical case is fan speed control in which the torque required varies as the speed squared. For this case, equating the motor torque to the load torque results in:

$$\frac{3}{2} P \frac{I_2^2 r_2}{S \omega_e} = K_L \omega_e (1 - S)^2 \quad (15.6)$$

Solving for I_2^2 as a function of S and differentiating yields the result that the maximum value of I_2^2 (and hence of rotor loss) occurs at:

$$S = 1/3 \quad (15.7)$$

or at a speed of two-thirds of synchronous speed. If this worst case value is substituted back to find the maximum required value of I_2^2 and the result used to relate the maximum rotor loss to the rotor loss at rated slip, the result is

$$\frac{\text{Maximum rotor } I^2 r \text{ loss}}{\text{Rated rotor } I^2 r \text{ loss}} = \frac{(4/27)}{S_{rated}(1 - S_{rated})} \quad (15.8)$$

where S_{rated} equals rated slip. Figure 15.6 illustrates this result and from this curve it is clear that, to avoid excessive rotor heating at reduced speed with a fan load, it is essential that the rated slip be in the range 0.25 – 0.35 to avoid overheating. While the use of such high slip machines will avoid rotor overheating, it does not improve the efficiency. The low efficiency associated with high slip operation is inherent in all induction machines and the high slip losses implies that these machine will generally be large and bulky.

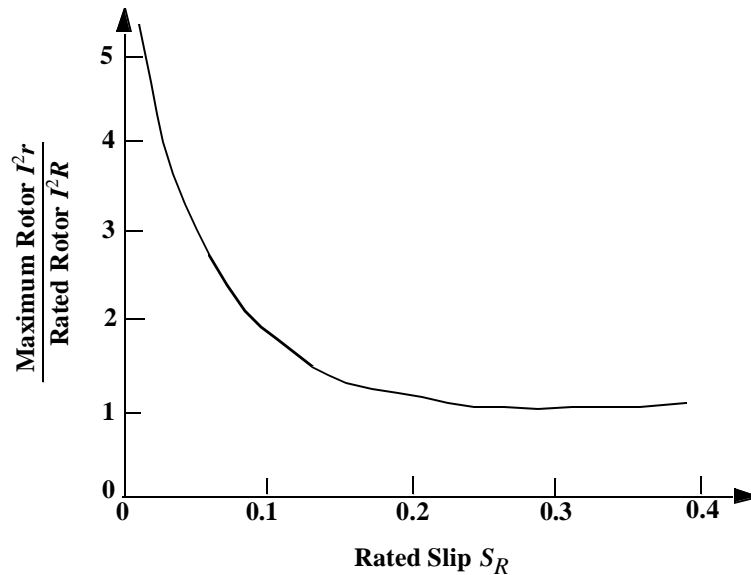


Figure 15.6 Worst case rotor heating for induction motor with a fan load

As noted previously, speed stability is an inherent problem in voltage-controlled induction motor drives at low speeds. This is a result of the near coincidence of the motor torque characteristic and the load characteristic at low speed. The problem occurs primarily when the intersection of the motor torque characteristic and the load characteristic occurs near or below the speed of maximum motor torque (see point B in Figure 15.5).

Reduced voltage operation of an induction machine will result in lower speed but this requires increased slip and the rotor $I^2 r$ losses are accordingly

increased. This type of high slip drive is therefore limited in application to situations where the high losses and low efficiency are acceptable and, generally, where the speed range is not large. Such drives are today generally limited to relatively low power ratings because of cooling problems.

The voltage controller of Figure 15.2, however, remains popular for motor starting applications. Motor starters are intended to provide a reduction in starting current. Inverse parallel thyristor starters reduce the current by the voltage ratio and the torque by the square of the ratio. Unlike autotransformer or reactance starters which have only one or two steps available, an inverse parallel thyristor starter can provide step-less and continuous “reactance” control. These electronic starters are often fitted with feedback controllers which allow starting at a preset constant current, although simple timed starts are also available. Some electronic starters are equipped to short-out the inverse parallel thyristor at the end of the starting period to eliminate the losses due to forward voltage drop during running. Other applications include “energy savers” which vary the voltage during variable-load running conditions to improve efficiency.

15.3 Thyristor Based Load-Commutated Inverter Synchronous Motor Drives

The basic thyristor based load-commutated inverter synchronous motor drive system is shown in Figure 15.7. In this drive, two static converter bridges are connected on their DC side by means of a so-called DC link having only a n inductor on the DC side. The line side converter ordinarily takes power from a constant frequency bus and produces a controlled DC voltage at its end of the DC link inductor. The DC link inductor effectively turns the line side converter into a current source as seen by the machine side converter. Current flow in the line side converter is controlled by adjusting the firing angle of the bridge and by natural commutation of the AC line.

The machine side converter normally operates in the inversion mode. Since the polarity of the machine voltage must be instantaneously positive as the current flows into the motor to commutate the bridge thyristors, the synchronous machine must operate at a sufficiently leading power factor to provide the volt-seconds necessary to overcome the internal reactance opposing the transfer of current from phase to phase (commutating reactance). Such load EMF-dependent commutation is called *load commutation*. As a result of the action of the

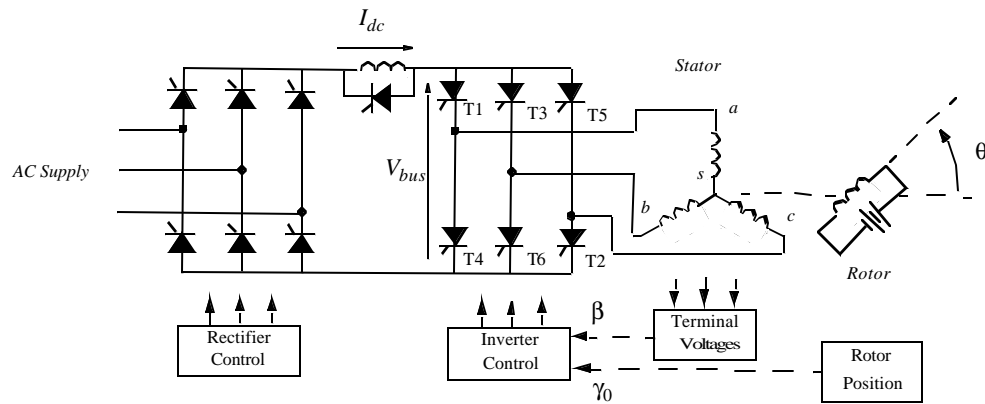


Figure 15.7 Load commutated inverter synchronous motor drive

link inductor, such an inverter is frequently termed a *naturally commutated current source inverter*.

Figure 15.8 illustrates typical circuit operation. Inverter thyristors 1-6 fire in sequence, one every 60 electrical degrees of operation, and the motor currents form balanced three-phase quasi-rectangular waves. The electrical angles shown in Figure 15.8 pertain to commutation from thyristor 1 to 3. The instant of commutation of this thyristor pair is defined by the *phase advance angle* β relative to the machine terminal voltage V_{ab} . Once thyristor 3 is switched on, the machine voltage V_{ab} forces current from phase *a* to phase *b*. The rate of rise of current in thyristor 3 is limited by the commutating reactance, which is approximately equal to the subtransient reactance of the machine.

During the interval defined by the *commutation overlap angle* μ the current in thyristor 3 rises to the DC link current I_{dc} while the current in thyristor 1 falls to zero. At this instant, V_{ab} appears as a negative voltage across thyristor 1 for a period defined as the *commutation margin angle* Δ . The angle Δ defines, in effect, the time available to the thyristor to recover its blocking ability before it must again support forward voltage. The corresponding time $T_r = \Delta/\omega$ is called the *recovery time* of the thyristor. The phase advance angle β is equal to the sum of μ plus Δ . The angle β is defined with respect to the motor terminal voltage. In practice it is useful to define a different angle γ_0 measured with respect to the internal EMF of the machine. This angle is called the *firing angle*. Since the internal EMFs are simply equal to the time rate of change of the rotor flux linking the stator windings, the firing angle γ_0 can be located

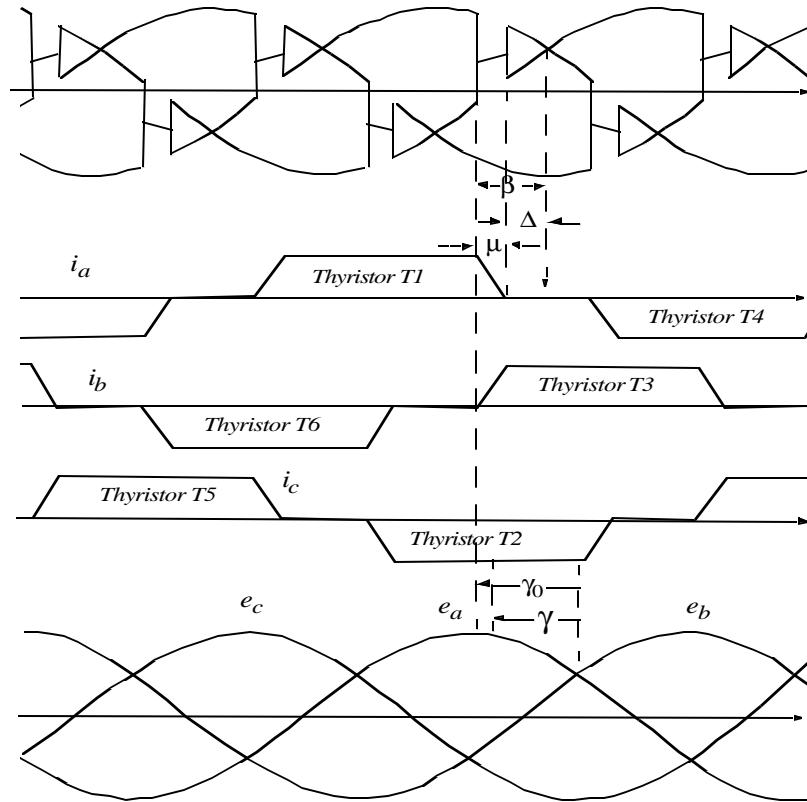


Figure 15.8 Load commutated synchronous motor waveforms and control variables

physically as the instantaneous position of the salient poles of the machine, i.e. the d -axis of the machine relative to the magnetic axis of the outgoing phase that is undergoing commutation (in case phase a). Hence, in general, the system is typically operated in a self-synchronous mode where the output shaft position (or a derived position-dependent signal) is used to determine the applied stator frequency and phase angle of current.

A fundamental component per-phase phasor diagram of Figure 15.9 illustrates this requirement. In this figure the electrical angle γ is the equivalent of γ_0 but corresponds to the phase displacement of the fundamental component of stator current with respect to the EMF. Spatially, γ corresponds to 90° minus the angle between the stator and rotor MMFs and may be called the *MMF*

angle. A large leading MMF angle γ is clearly necessary to obtain a leading terminal power factor angle ϕ .

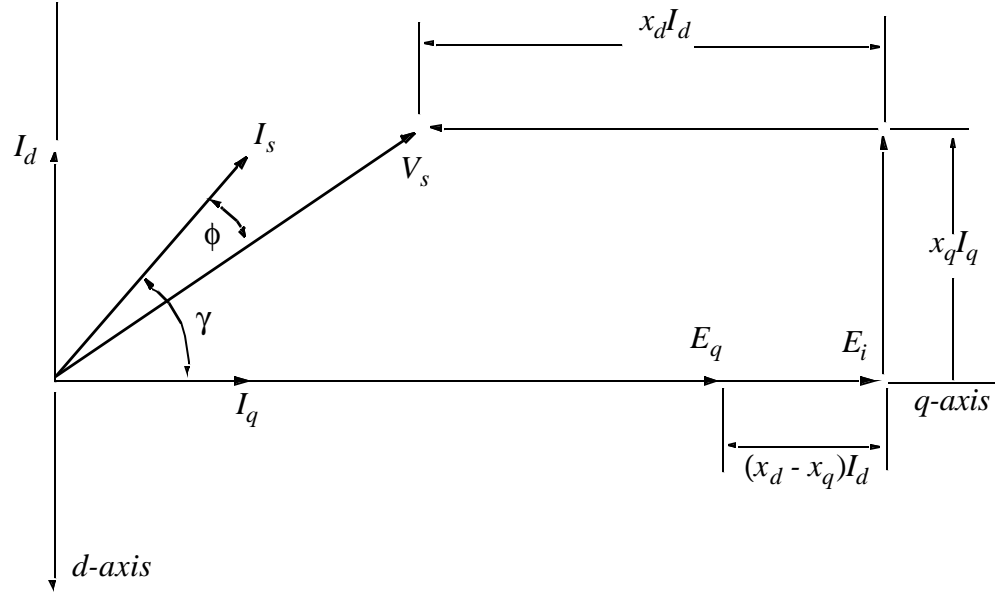


Figure 15.9 Phasor diagram for load commutated inverter synchronous motor drive

15.3.1 Torque Production in a Load Commutated Inverter Synchronous Motor Drive

The average torque developed by the machine is related to the power delivered to the internal EMF E_i and, from Figure 15.9, can be written as:

$$T_e = \frac{3E_i I_s \cos \gamma}{\omega_{rm}} \quad (15.9)$$

where ω_{rm} is the mechanical speed (i.e. $\omega_{rm} = 2\omega_e/P$ for steady state conditions). The angle γ is the electrical angle between the internal EMF and the fundamental component of the corresponding phase current and is located in Figure 15.8 for the c phase. It should be noted that this angle is very close the angle γ_0 which corresponds to a physical angle which can be set by means of a suitably located position sensor.

In general, E_i is speed-dependent,

$$E_i = \frac{P}{2} \omega_{rm} \lambda_{af} \quad (15.10)$$

and the apparent speed dependence vanishes whereupon Equation (15.9) takes the form,

$$T_e = \frac{3}{2} P \lambda_{af} I_s \cos \gamma \quad (15.11)$$

where λ_{af} is rms value of the field flux linking a stator phase winding. Thus, for a fixed value of the internal angle γ , the system behaves very much like a DC machine and its steady state torque control principles are possible.

15.3.2 Torque Capability Curves

One useful measure of drive performance is a curve showing the maximum torque available over its entire speed range. A synchronous motor supplied from a variable-voltage, variable-frequency supply will exhibit a torque-speed characteristic similar to that of a DC shunt motor. If field excitation control is provided, operation above base speed in a field-weakened mode is possible and is used widely. The upper speed limit is dictated by the required commutation margin time of the inverter thyristors.

Figure 15.10 is a typical capability curve assuming operation at constant-rated DC link current, at rated (maximum) converter DC voltage above rated speed and with a commutation margin time Δ/ω_o of 26.5 ms corresponding to $\Delta = 12^\circ$ at 50 Hz. At very low speeds, where the commutation time is of the order of the motor transient time constants, the machine resistances make up a significant part of the commutation impedance. The firing angle must subsequently be increased to provide sufficient volt-seconds for commutation as shown by the companion curves of Figure 15.11. The resulting increase in internal power factor angle reduces the torque capability. At intermediate speeds the margin angle can be reduced to values less than 12° to maintain 26.5 ms margin time and slightly greater than rated torque can be produced.

Above rated speed the inverter voltage is maintained constant and the drive, in effect, operates in the constant kilovolt-ampere mode. The DC inverter voltage reaches the maximum value allowed by the device ratings and the maximum output of the rectifier. Although Figure 15.10 shows a weakening of the field in the high-speed condition, the reduction is not as great as the inverse speed relationship required for constant horsepower operation. This again is a consequence of the constant commutation margin angle control. Since the margin angle increases with speed, i.e. frequency, to maintain the same margin time, the corresponding increase in power factor angle results in a

greater demagnetizing component of stator MMF This offsets partly the need to weaken the field in the high-speed region.

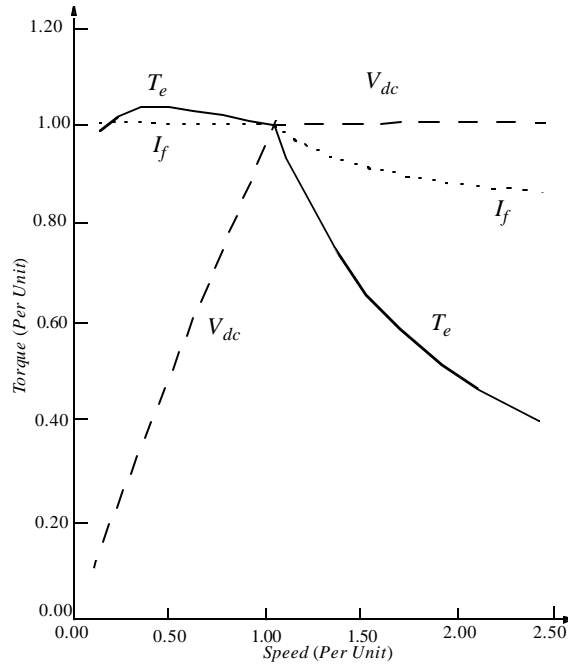


Figure 15.10 Capability curve of a load commutated inverter synchronous motor drive with constant DC link current and fixed commutation margin time, field weakening operation above one p.u. speed assumes operation at constant DC link voltage

15.3.3 Constant Speed Performance

When the DC link current is limited to its rated value, the maximum torque can be obtained from the capability curve (Figure 15.10). However, operation below maximum torque requires a reduction in the DC link current. When the field current is adjusted to keep the margin angle Δ at its limiting value, the curves of Figure 15.12 result. It can be noted that the torque is now essentially a linear function of DC link current so that the DC link current command becomes, in effect, the torque command.

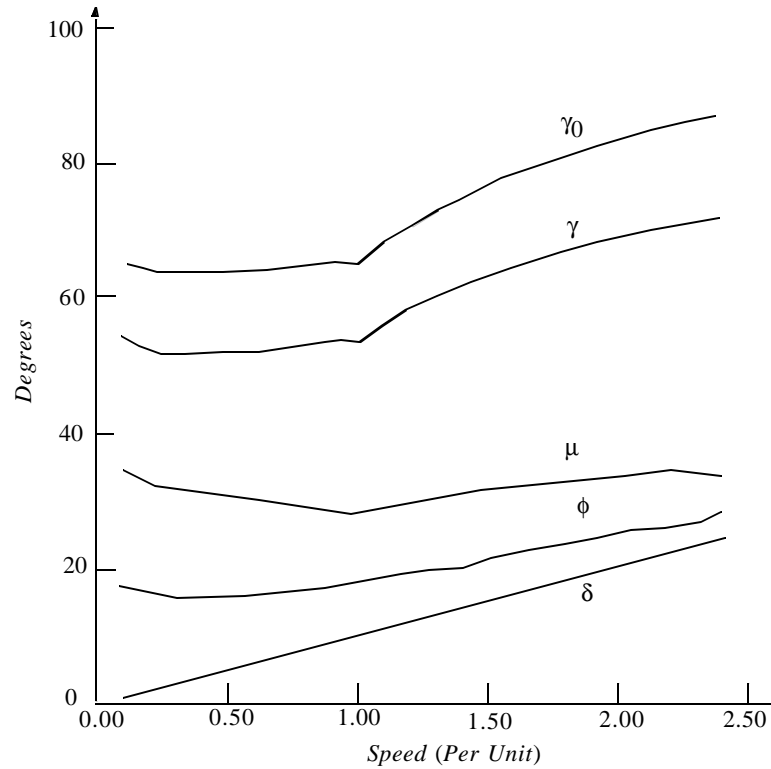


Figure 15.11 Characteristic electrical control angles for load commutated synchronous motor drive

15.3.4 Control Considerations

Direct control of γ_0 by use of a rotor position sensor has traditionally been applied in load commutated inverter drives but has largely been replaced by schemes using terminal voltage and current sensing to indirectly control γ . The basic principle is to use Eq. (15.11) as the control equation. If terminal voltage across the machine and the dc link current are measured, then if γ is held constant the dc link current required for given torque is

$$I_s = \frac{T_e \omega_{rm}}{3E_i \cos \gamma} \quad (15.12)$$

The dc link current that must be supplied can be determined from the current I_s by relating the fundamental component of a quasi-rectangular motor phase cur-

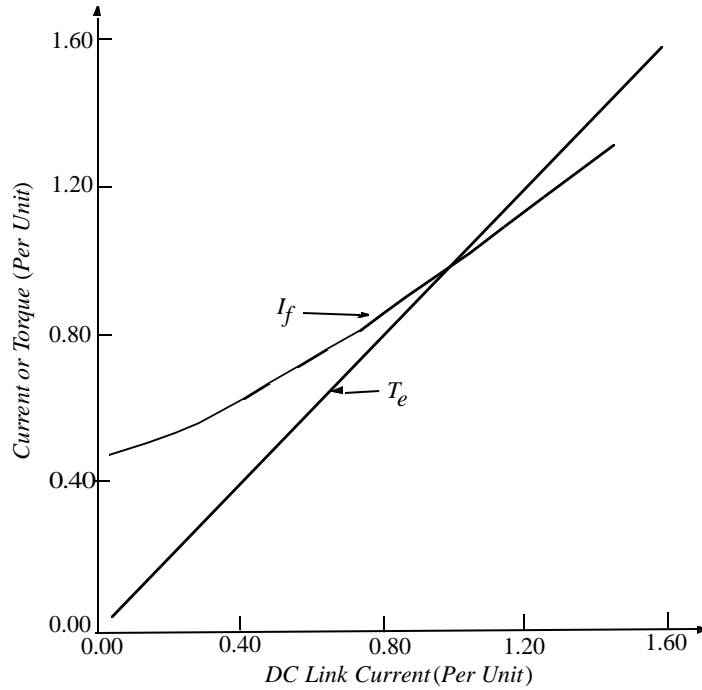


Figure 15.12 DC field current required to produce a linear variation of Torque with DC link current, operation at rated speed, margin angle $\Delta = 10^\circ$

rent (see Figure 15.8) to its peak value I_{dc} . The result is, with reasonable approximation

$$I_{dc} = \frac{\pi}{\sqrt{6}} I_s \quad (15.13)$$

The internal rms phase voltage E_i can be calculated by considering the reactive drop and is obtained from Figure 15.9. Control is implemented such that the machine side converter is controlled to maintain either γ or β constant while the line side converter is controlled to provide the correct dc link current to satisfy Eq. (15.12) [

Direct control of the commutation margin angle Δ (more correctly, the margin time Δ/ω_o where ω_o is the motor angular frequency) has the advantage of causing operation at the highest possible power factor and hence gives the best utilization of the machine windings. The waveforms in Figure 15.11 also demonstrate that changes in the commutation overlap angle μ resulting from current or speed changes produce significant differences between the actual value of γ and the ideal value γ_o . For this reason, compensators are required in direct

γ controllers. This compensation is automatic in systems based on controlling the margin angle Δ .

15.4 Transistor Based Variable-Frequency Induction Motor Drives

15.4.1 Introduction

Variable-frequency AC drives are now available from fractional kilowatts to very large sizes, e.g. to 15 000 kW for use in electric generating stations. In large sizes, naturally commutated converters are more common, usually driving synchronous motors. However, in low to medium sizes (up to approximately 750kW) transistor based PWM voltage source converters driving induction motors are almost exclusively used. Figure 15.13 illustrates the basic power circuit topology of the voltage source inverter. Only the main power-handling devices are shown; auxiliary circuitry such as snubbers or commutation elements are excluded.

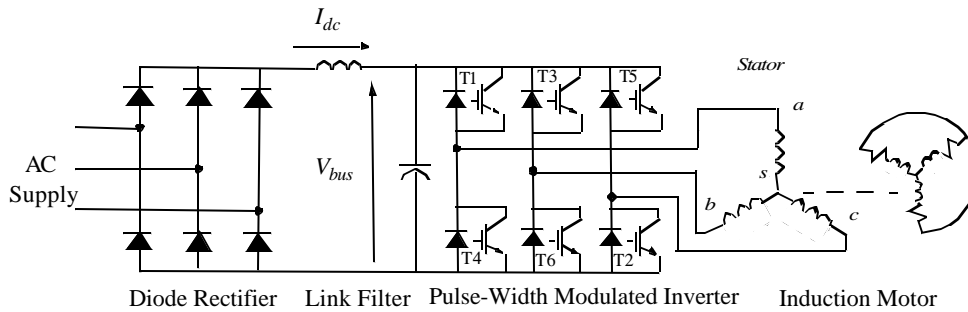


Figure 15.13 Basic circuit topology of pulse-width modulated inverter drive

The modern strategy for controlling the AC output of such a power electronic converters is the technique known as *Pulse-Width Modulation* (PWM), which varies the *duty cycle* (or *mark-space* ratio) of the converter switch(es) at a high switching frequency to achieve a target average low frequency output voltage or current. In principle, all modulation schemes aim to create trains of switched pulses which have the same fundamental volt-second average (i.e. the integral of the waveform over time) as a target reference waveform at any instant. The

major difficulty with these trains of switched pulses is that they also contain unwanted harmonic components which should be minimized.

Three main techniques for PWM exist. These alternatives are:

1. switching at the intersection of a target reference waveform and a high frequency triangular carrier (*Double Edged Naturally Sampled Sine-Triangle PWM*).
2. switching at the intersection between a regularly sampled reference waveform and a high frequency triangular carrier (*Double Edged Regular Sampled Sine-Triangle PWM*).
3. switching so that the amplitude and phase of the target reference expressed as a vector is the same as the integrated area of the converter switched output over the carrier interval (*Space Vector PWM*).

Many variations of these three alternatives have been published, and it sometimes can be quite difficult to see their underlying commonality. For example, the space vector modulation strategy, which is often claimed to be a completely different approach to modulation, is really only a variation of regular sampled PWM which specifies the same switched pulse widths but only places them a little differently in each carrier interval.

15.4.2 Double Edged Naturally Sampled Sine-Triangle PWM

The most common form of PWM is the naturally sampled method in which a sine wave command is compared with a high frequency triangle as shown for one of three phases in Figure 15.14. Intersections of the commanded sine wave and the triangle produce switching in the inverter as shown in Figure 15.15. The triangle wave is common to all three phases. Figure 15.15(b) shows the modulation process in detail, expanded over a time interval of two subcycles, $\Delta T/2$. Note that because of switching action the potentials of all three phases are all equal making the three line to line voltages (and thus the motor phase voltages) zero. The width of these zero voltage intervals essentially provides the means to vary the fundamental component of voltage when the frequency is adjusted so as to realize constant volts/Hz (nearly constant stator flux) operation. A close inspection of Figure 15.14 indicates that this method does not fully utilize the available DC voltage since the sine wave command amplitude reaches the peak of the triangle wave only when the output line voltage is $2/\pi$ or 0.785 of the maximum possible value of V_{bus} . This deficiency can be

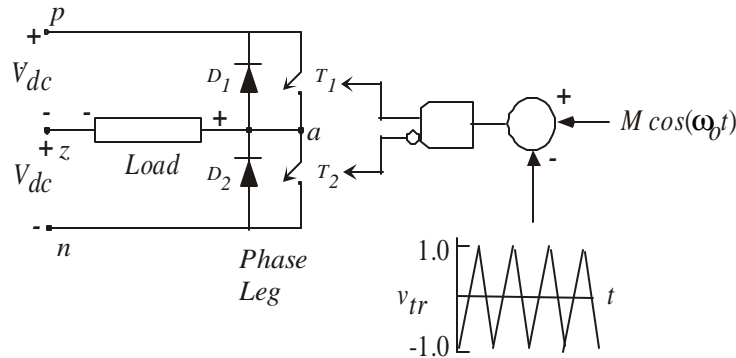


Figure 15.14 Control principle of naturally sampled PWM showing one of three phase legs

reduced by introducing a zero sequence third harmonic component command into each of the controllers. With a third harmonic amplitude of $1/6$ that of the sine wave command, the output can be shown to be increased to $(\sqrt{3})/2$ or $0.866V_{bus}$. Additional zero sequence harmonics can be introduced to further increase the output to $(\sqrt{3}\pi)/6$ or $0.907V_{bus}$. Further increases in voltage can only be obtained by introducing low frequency odd harmonic into the output waveform.

15.4.3 Double Edged Regular Sampled Sine-Triangle PWM

One major limitation with naturally sampled PWM is the difficulty of its implementation in a digital modulation system, because the intersection between the reference sinusoid and the triangular or saw-tooth carrier is defined by a transcendental equation and is complex to calculate. To overcome this limitation the modern alternative is to implement the modulation system using a “regular sampled” PWM strategy, where the low frequency reference waveforms are sampled and then held constant during each carrier interval. These sampled values are then compared against the triangular carrier waveform to control the switching process of each phase leg, instead of the sinusoidally varying reference.

The sampled reference waveform must change value at either the positive or positive/negative peaks of the carrier waveform, depending on the sampling strategy. This change is required to avoid instantaneously changing the reference during the ramping period of the carrier, which may cause multiple switch

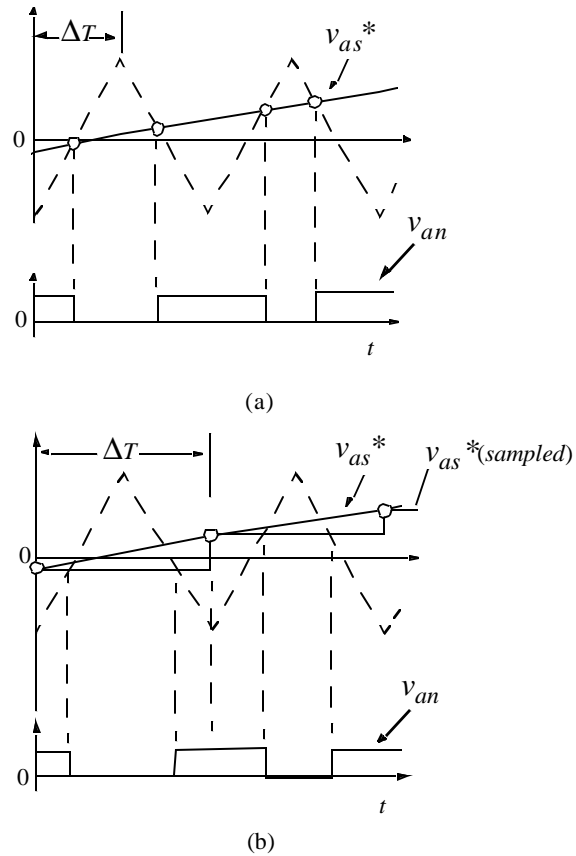


Figure 15.15 (a) Naturally sampled PWM and (b) symmetrically sampled PWM

transitions if it was allowed to occur. For a triangular carrier, sampling can be *symmetrical*, where the sampled reference is taken at either the positive or negative peak of the carrier and held constant for the entire carrier interval, or *asymmetrical*, where the reference is re-sampled every half carrier interval at both the positive and the negative carrier peak. The asymmetrical sampling is preferred since the update rate of the sampled waveform is doubled resulting in a doubling in the harmonic spectrum resulting from the PWM process. The phase delay in the sampled waveform can be corrected by phase advancing the reference waveform.

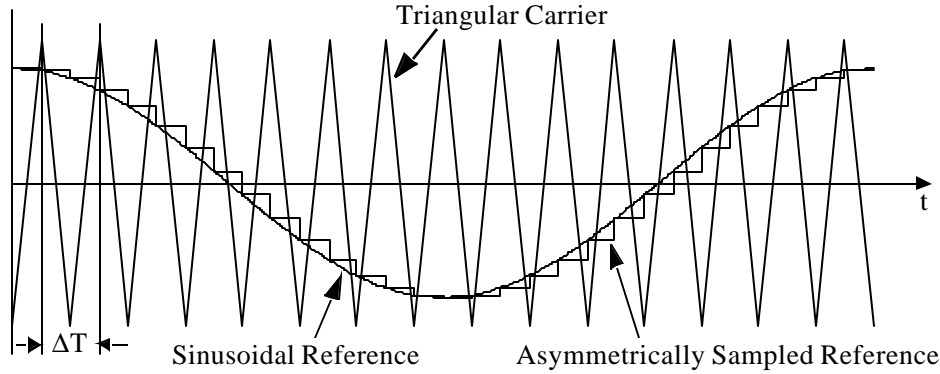


Figure 15.16 Regular asymmetrically sampled pulse width modulation

15.4.4 Space Vector PWM

In the mid 1980's a form of PWM called “Space Vector Modulation” (SVM) was proposed, which was claimed to offer significant advantages over natural and regular sampled PWM in terms of performance, ease of implementation and maximum transfer ratio [4], [5]. The principle of SVM is based on the fact that there are only 8 possible switch combinations for a three phase inverter. The basic inverter switch states are shown in Figure 15.17. Two of these states (SV_0 and SV_7) correspond to the short circuit discussed previously, while the other six can be considered to form stationary vectors in the d - q plane as shown in Figure 15.19. The magnitude of each of the six active vectors is,

$$V_m = \frac{2}{3}V_{bus} \quad (15.14)$$

corresponding to the maximum possible phase voltage. Having identified the stationary vectors, at any point in time, an arbitrary target output voltage vector \bar{V}_o can then be made up by the summation (“averaging”) of the adjacent *space vectors* within one switching period ΔT , as shown in Figure 15.19 for a target vector in the first 60° segment of the plane. Target vectors in the other five segments of the hexagon are clearly obtained in a similar manner.

For ease in notation, the d - q plane can be considered as being complex. The geometric summation shown in Figure 15.19 can then be expressed mathematically as

$$\frac{T_{SV1}}{(\Delta T/2)}\overline{SV_1} + \frac{T_{SV2}}{(\Delta T/2)}\overline{SV_2} = \bar{V}_o \quad (15.15)$$

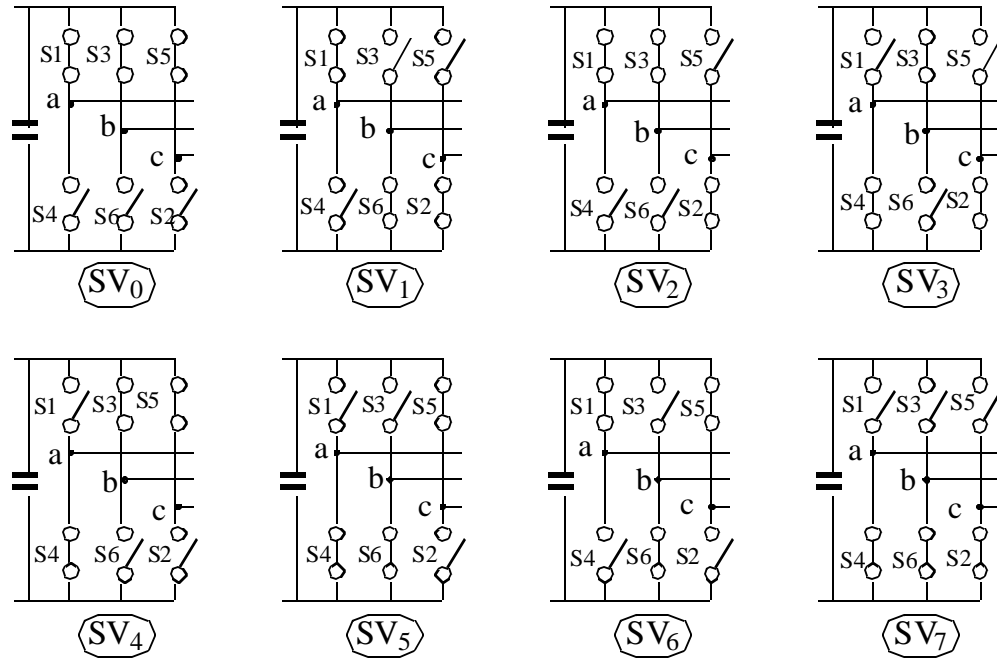


Figure 15.17 Eight possible phase leg switch combinations for a VSI

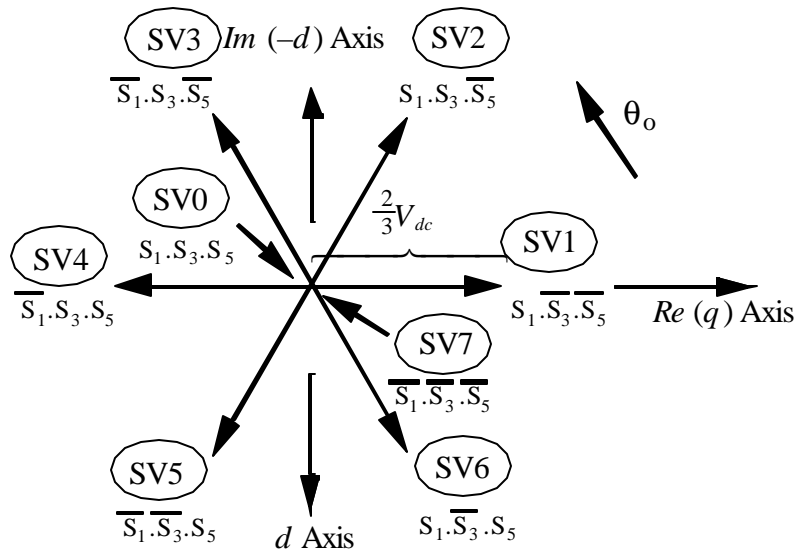


Figure 15.18 Location of the eight possible stationary voltage vectors for a VSI in the d - q (Re - Im) plane. Each vector has a length $(2/3)V_{bus}$

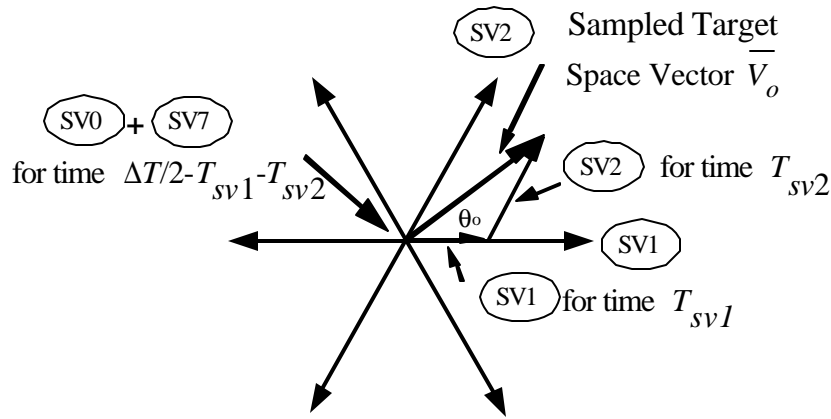


Figure 15.19 Creation of an arbitrary output target phasor by the geometrical summation of the two nearest space vectors

for each switching period of $\Delta T/2$. That is, each active space vector is selected for some interval of time which is less than the one-half carrier period. It can be noted that SVM is an intrinsically a regular sampled process, since in essence it matches the sum of two space vector volt-second averages over a half carrier period to a sampled target volt-second average over the (15.15)

$$T_{SV1}V_m \angle 0 + T_{SV2}V_m \angle \pi/3 = \left(\frac{\Delta T}{2}\right)V_o \angle \theta_o \quad (15.16)$$

or in cartesian form:

$$T_{SV1}V_m + T_{SV2}V_m \left(\cos \frac{\pi}{3} + j \sin \frac{\pi}{3} \right) = V_o (\cos \theta_o + j \sin \theta_o) \frac{\Delta T}{2} \quad (15.17)$$

Equating real and imaginary components yields the solution,

$$T_{SV1} = \frac{V_o \sin\left(\frac{\pi}{3} - \theta_o\right)}{V_m \sin \frac{\pi}{3}} \frac{\Delta T}{2} \quad (\text{active time for SV1}) \quad (15.18)$$

$$T_{SV2} = \frac{V_o \sin(\theta_o)}{V_m \sin \frac{\pi}{3}} \frac{\Delta T}{2} \quad (\text{active time for SV2}) \quad (15.19)$$

Since $0 \leq T_{SV1}, T_{SV2} \leq \Delta T/2$, the maximum possible magnitude for V_o is V_m , which can occur at $\theta_o = 0^\circ$ or $\pi/3$.

In addition a further constraint is that the sum of the active times for the two space vectors obviously cannot exceed the half carrier period, i.e. $T_{SV1} + T_{SV2} \leq \Delta T/2$. From simple geometry, the limiting case for this occurs at $\theta_o = \pi/6$, which means,

$$\frac{T_{SV1} + T_{SV2}}{\left(\frac{\Delta T}{2}\right)} = \left(\frac{V_o}{V_m}\right) \frac{2 \sin \frac{\pi}{6}}{\sin \frac{\pi}{3}} \leq 1 \quad (15.20)$$

and this relationship constrains the maximum possible magnitude of V_o to

$$V_o = V_m \sin\left(\frac{\pi}{3}\right) = \frac{1}{\sqrt{3}} V_{bus} \quad (15.21)$$

Since V_o is the magnitude of the output *phase* voltage, the maximum possible *l-l* output voltage using SVM must equal:

$$V_{o(l-l)} = \sqrt{3} V_o = V_{bus} \quad (15.22)$$

This result represents an increase of $2/(\sqrt{3})$ or 1.1547 compared to regular sampled PWM (Section 15.4.2) but is essentially the same when zero sequence harmonics are added to the voltage command as was previously discussed.

15.4.5 Constant Volts/Hertz Induction Motor Drives

The operation of induction machines in a constant volts per hertz mode back to the late fifties and early sixties but were limited in their low speed range[6]. Today constant volt per hertz drives are built using PWM-IGBT-based inverters of the types discussed in Sections 15.4.2 to 15.4.4 and the speed range has widened to include very low speeds [7] although operation very near zero speed (less than 1 Hz) remains as a challenge mainly due to inverter non-linearities at low output voltages.

Ideally, by keeping a constant V/f ratio for all frequencies the nominal torque-speed curve of the induction motor can be reproduced at any frequency as discussed in Section 15.2.2. Specifically if stator resistance is neglected and keeping a constant slip frequency the steady state behavior of the induction machine can be characterized as an impedance proportional to frequency. Therefore, if the V/f ratio is kept constant the stator flux, stator current, and

torque will be constant at any frequency. This feature suggests that to control the torque one needs to simply apply the correct amount of V/Hz to stator windings. This simple, straight forward approach, however, does not work well in reality due to several factors, the most important ones being

- 1) Effect of supply voltage variations
- 2) Influence of stator resistance
- 3) Non-ideal torque/speed characteristic (effects of slip)
- 4) Non-linearities introduced by the PWM inverter.

Low frequency operation is the particularly difficult to achieve since these effects are most important at low voltages. Also, the non-linearities within the inverter, if not adequately compensated, yield highly distorted output voltages which, in turn, produces pulsating torques that lead to vibrations and increased acoustic noise.

In addition to these considerations, a general purpose inverter must accommodate a variety of motors from different manufacturers. Hence it must compensate for the above mentioned effects regardless of machine parameters. The control strategy must also be capable of handling parameter variations due to temperature and/or saturation effects. This fact indicates that in a true “general purpose” inverter it is necessary to include some means to estimate and/or measure some of the machine parameters. Another aspect that must be considered in any practical implementation deals with the DC bus voltage regulation, which, if not taken into account, may lead to large errors in the output voltage.

Because general purpose drives are cost sensitive it is also desired to reduce the number of sensing devices within the inverter. Generally speaking only the do link inverter voltage and current are measured, hence the stator current and voltage must be estimated based only on these measurements. Speed encoders or tachometers are not used because they add cost as well as reduce system reliability.

Other aspects that must be considered in the implementation of an “ideal constant V/f drive” relate to:

- a) current measurement and regulation,
- b) changes in gain due to pulse dropping in the PWM inverter,

- c) instabilities due to poor volt-second compensation that result in lower damping. This problem is more important in high efficiency motors, and
- d) quantization effects in the measured variables.

Another aspect that must be carefully taken into account is the quantization effect introduced by the A/D converters used for signal acquisition. A good cost to resolution compromise seems to be the use of 10 bit converters. However, a high performance drive is likely to require 12 bit accuracy.

15.4.6 Required Performance of Control Algorithms

The key features of a typical control algorithm, is defined as follows:

- a) Open loop speed accuracy: 0.3-0.5% (5.4 to 8.2 rpm)
- b) Speed control region: 1-30 to 1:50 (60 - 1.2 Hz to 60 - 2 Hz)
- c) Torque range: 0 to 150%
- c) Output voltage accuracy: 1-2% (1.15 - 2.3 volts)
- d) Speed response with respect to load changes: less than 2 seconds
- e) Self commissioning capabilities: parameter estimation error less than 10%
- f) Torque-slip linearity: within 10-15%
- g) Energy saving mode: for no-load operation the power consumed by the motor must be reduced by 20% with respect to the power consumed at full flux and no load.

Current sensors are normally of the open-loop type and their output needs to be compensated for offset and linearity. In addition the DC link bus voltage is typically measured. The switching frequency for the PWM is fixed at typically 10 to 12 kHz.

It is frequently also required to measure or estimate the machine parameters used to implement the control algorithms. In such cases it is assumed that the number of poles, rated power, rated voltage, rated current, and rated frequency are known.

15.4.7 Compensation for Supply Voltage Variations

In an industrial environment, a motor drive is frequently subjected to supply voltage fluctuations which, in turn, imposed voltage fluctuations on the DC

link of the inverter. If these variations are not compensated for, the motor will be impressed with either an undervoltage or an overvoltage which produces excessive I^2r loss or excessive iron loss respectively. The problem can be avoided if the DC link voltage is measured and the voltage command V_1^* adjusted to produce a modified command V_1^{**} such that

$$V_1^{**} = \left(\frac{V_{busR}}{V_{bus}} \right) V_1^* \quad (15.23)$$

where V_{busR} is the rated value of bus voltage.

15.4.8 I_r Compensation

A simple means to compensate for the resistive drop is to boost the stator voltage by $I_1^* r_1$ (voltage proportional to the current magnitude) and neglect the effect of the current phase angle. To avoid the direct measurement of the stator current this quantity can be estimated from the magnitude of the dc-link current [8]. In this paper a good ac current estimate was demonstrated at frequencies as low as 2 Hz but the system requires high accuracy in the dc-link current measurement making it impractical for low cost applications. A robust I_r boost method must include both magnitude and phase angle compensation. Typically currents of two phases must be measured with the third current inferred since the currents sum to zero. In either case the value of the stator resistance must be known.

The value of the stator resistance can be estimated by using any one of several known techniques [9]–[11]. Unfortunately these parameter estimation techniques require knowing the rotor position or velocity and the stator current. An alternate method of 'boosting' the stator voltage at low frequencies is presented in [12]. Here the V/f ratio is adjusted by using the change in the sine of the phase angle of motor impedance. This approach also requires knowing the rotor speed and it is also dependent on the variation of the other machine parameters. Its practical usefulness is questionable because of the technical difficulty of measuring phase angles at frequencies below 2 Hz.

Constant Volts/Hz control strategy is typically based on keeping the stator flux-linkage magnitude constant and equal to its rated value. Using the steady state equivalent circuit of the induction motor, shown in Figure 15.3, an expression for stator voltage compensation for resistive drop can be shown to be

$$V_1 = \frac{\sqrt{2}}{3} I_{1(Re)} \cdot \hat{R}_1 + \sqrt{\frac{V_{1R} f_e}{f_R} + \frac{2}{9} (i_{1(re)} \cdot \hat{R}_1)^2 - (I_1 \hat{R}_1)^2} \quad (15.24)$$

where V_{1R} is the base (rated) rms phase voltage at base frequency, f_R is the rated frequency in Hertz, \hat{R}_1 is the estimated value of resistance, I_s is the rms current obtained on a instantaneous basis by,

$$I_s = \sqrt{\frac{2}{3}} \sqrt{i_a(i_a + i_c) + i_c^2} \quad (15.25)$$

and $I_{1(Re)}$ is the real component of rms stator current obtained from

$$I_{1(Re)} = i_a \left[\cos \theta_e - \cos \left(\theta_e - 2\frac{\pi}{3} \right) \right] + i_c \left[\cos \left(\theta_e + 2\frac{\pi}{3} \right) - \cos \left(\theta_e - 2\frac{\pi}{3} \right) \right] \quad (15.26)$$

where i_a and i_c are two of the instantaneous three phase stator currents $\theta_e = \omega_e t$ and the cosine terms are obtained from the voltage command signals. The estimated value of resistance can be obtained either by a simple dc current measurement corrected for temperature rise or by a variety of known methods[13]–[15]. Derivation details of these equations are found in [16]. Given the inherently positive feedback characteristic of an Ir boost algorithm it is necessary to stabilize the system by introducing a first order lag in the feedback loop (low-pass filter).

15.4.9 Slip Compensation

By its nature, the induction motor develops its torque as a rotor speed slightly lower than synchronous speed (effects of slip). In order to achieve a desired speed, the applied frequency must therefore be increased by an amount equal to the slip frequency. The usual method of correction is to assume a linear relationship exists between torque and speed in the range of interest, Hence, the slip can be compensated by knowing this relationship. This approximation gives good results as long as the breakdown torque is not approached. However, for high loads the relationship becomes non-linear. Ref. [16] describes a correction which can be used for high slip,

$$f_{slip} = \frac{1}{2 - A \cdot P_{gap}} \left\{ \sqrt{(f_e^*)^2 + \frac{S_m S_{linear}}{S_R} \cdot P_{gap} - B \cdot P_{gap}^2} - f_e^* \right\} \quad (15.27)$$

where f_e^* is the external command frequency and,

$$A = \frac{P}{4\pi S_{bd} T_{bd} f_R} \quad (15.28)$$

and

$$B = \left(\frac{P}{4\pi T_{bd}} \right)^2 \quad (15.29)$$

and P is the number of poles. The slope of the linear portion of the torque–speed curve is given by

$$S_{linear} = \left(\frac{P}{\pi} \right) \frac{S_R f_R}{T_R} \quad (15.30)$$

Finally the air gap power is

$$P_{gap} = 3V_1 I_1 (pf) - 3I_1^2 \hat{R}_1 - P_{core} \quad (15.31)$$

where P_{core} at rated frequency can be obtained from

$$P_{coreR} = P_{inR} \left(1 - \frac{\eta_R}{1 - S_R} \right) - 3I_{1R}^2 \hat{R}_1 \quad (15.32)$$

where the caret “^” denotes an estimate of the quantity. The quantities $S_R, f_R, \eta_R, I_{1R}, P_{inR}$ and T_R are the rated values of slip frequency, line frequency, efficiency, stator current, input power and torque respectively. All of these quantities can be inferred from the nameplate data.

15.4.10 Volt-Second Compensation

One of the main problems in open-loop controlled PWM-VSI drives is the non-linearity caused by the non-ideal characteristics of the power switches. The most important non-linearity is introduced by the necessary blanking time to avoid short circuiting the DC link during the commutations. To guarantee that both switches are never on simultaneously a small time delay is added to

the gate signal of the turning-on device. This delay, added to the device's inherent turn-on and turn-off delay times, introduces a magnitude and phase error in the output voltage[17]. Since the delay is added in every PWM carrier cycle the magnitude of the error grows in proportion to the switching frequency, introducing large errors when the switching frequency is high and the total output voltage is small.

The second main non-linear effect is due to the finite voltage drop across the switch during the on-state[18]. This introduces an additional error in the magnitude of the output voltage, although somewhat smaller, which needs to be compensated.

To compensate for the dead-time in the inverter it is necessary to know the direction of the current and then change the reference voltage by adding or subtracting the required volt-seconds. Although in principle this is simple, the dead time also depends on the magnitude and phase of the current and the type of device used in the inverter. The dead-time introduced by the inverter causes serious waveform distortion and fundamental voltage drop when the switching frequency is high compared to the fundamental output frequency. Several papers have been written on techniques to compensate for the dead time[17],[19]-[21].

Regardless of the method used, all dead time compensation techniques are based on the polarity of the current, hence current detection becomes an important issue. This is specially true around the zero-crossings where an accurate measurement is needed to correctly compensate for the dead time. Current detection becomes more difficult due to the PWM noise and because the use of filters introduces phase delays that needed to be taken into account.

The name “dead-time compensation” often misleads since the actual dead time, which is intentionally introduced, is only one of the elements accounting for the error in the output voltage, for this reason here it is referred as volt-second compensation. The volt-second compensation algorithm developed is based on the average voltage method. Although this technique is not the most accurate method available it gives good results for steady state operation. Figure 15.20 shows idealized waveforms of the triangular and reference voltages over one carrier period. It also shows the gate signals, ideal output voltage, and pole voltage for positive current. For this condition, the average pole voltage over one period can be expressed by:

$$\begin{aligned} \langle v_{an} \rangle = & V_{bus} \left(\frac{1}{2} + \frac{V^* \cos \theta}{V_{bus}} \right) - \left(\frac{t_d + t_{on} - t_{off}}{T_c} \right) (V_{bus} - V_{sat} + V_d) \\ & - \left(\frac{V_{sat} - V_d}{V_{bus}} \right) V^* - \left(\frac{V_{sat} + V_d}{2} \right) \end{aligned} \quad (15.33)$$

where:

$\langle v_{an} \rangle$: average output phase voltage with respect to negative dc bus over one switching interval,

V_{sat} : device saturation voltage,

T_c : carrier period,

V_{bus} : DC link bus voltage,

t_d : dead time,

t_{on} : turn-on delay time,

t_{off} : turn-off delay time,

V_d : diode forward voltage drop..

The first term in Eq. (15.33) represents the ideal output voltage and the remainder of the terms are the errors caused by the non-ideal behavior of the inverter. A close examination of the error terms shows that the first and last terms will be rather large with the middle term being much smaller. Hence one can approximate the voltage error by

$$\Delta V \approx \frac{t_d + t_{on} - t_{off}}{T_c} (V_{bus} - V_{sat} + V_d) + \frac{V_{sat} + V_d}{2} \quad (15.34)$$

and the output voltage can be expressed as

$$v_{an} \approx V_{bus} \left(\frac{1}{2} + \frac{V^* \cos \theta}{V_{bus}} \right) - \Delta V \quad (15.35)$$

if the current is positive and

$$v_{an} \approx V_{bus} \left(\frac{1}{2} + \frac{V^* \cos \theta}{V_{bus}} \right) + \Delta V \quad (15.36)$$

if the current is negative. Since the three motor phase voltage must add to zero the voltage of phase a with respect to the motor stator neutral s is therefore,

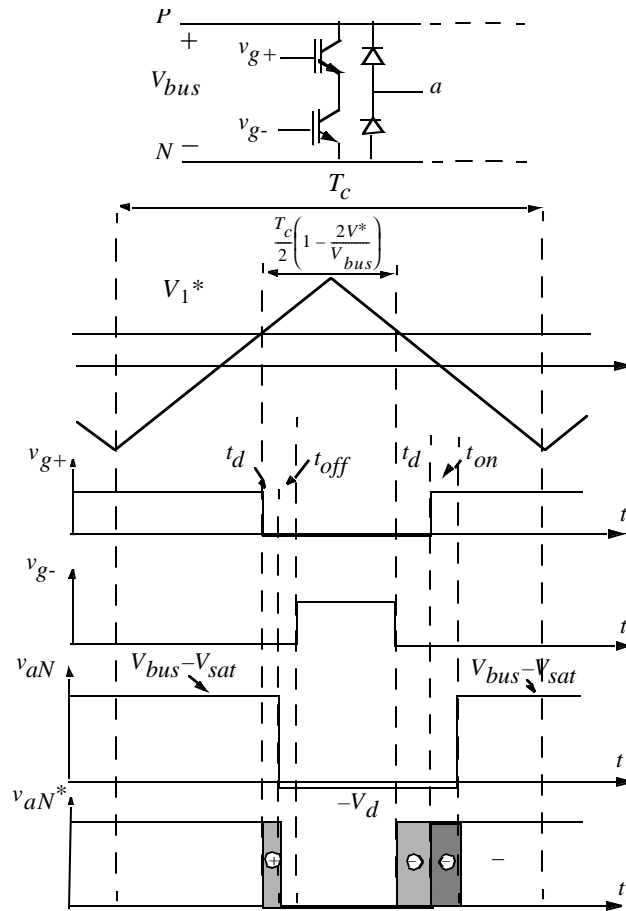


Figure 15.20 PWM voltage waveforms for positive current

$$v_{as} = \frac{2}{3}v_{an} - \frac{1}{3}v_{bn} - \frac{1}{3}v_{cn} \quad (15.37)$$

The voltages of the remaining two phase voltage are obtain in similar manner.

As shown in Figure 15.20, the voltage error corresponds to the difference in areas between the commanded voltage and the actual voltage. The (+) and (-) signs in the bottom trace indicate that in which part of the cycle there is a gain or loss of voltage. The algebraic sum of these areas gives the average error over a pulse period. The voltage error can be corrected either on a per pulse basis or, less accurately, on a per cycle basis. The compensation algorithm is thus based on commanding a voltage modified by $\pm\Delta V$ depending upon the

polarity of the current. An overall volts/Hertz control scheme including IR , slip and volt-second compensation is shown in Figure 15.21[16].

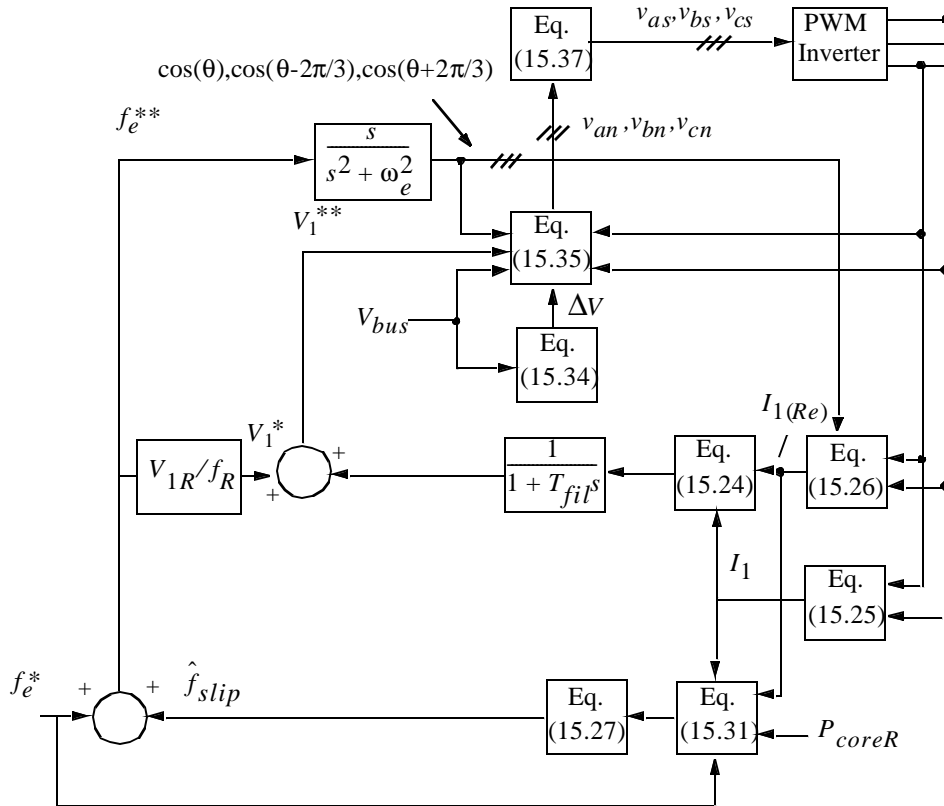


Figure 15.21 Complete volts per hertz induction motor speed controller incorporating IR , slip, DC bus and volt-second compensation

15.5 Field Orientation

15.5.1 Complex Vector Representation of Field Variables

Although the large majority of variable speed applications require only speed control in which the torque response is only of secondary interest, more challenging applications such a traction applications, servomotors and the like depend critically upon the ability of the drive to provide a prescribed torque whereupon the speed becomes the variable of secondary interest. The method of torque control in ac machines is called either *vector control* or, alternatively

field orientation. Vector control refers to the manipulation of terminal currents, flux linkages and voltages to affect the motor torque while field orientation refers to the manipulation of the field quantities within the motor itself. Since it is common for machine designers to visualize motor torque production in terms of the air gap flux densities and MMFs instead of currents and fluxes which relate to terminal quantities, it is useful to begin first with a discussion of the relationship between the two viewpoints.

Consider, first of all, the equation describing the instantaneous position of the stator air gap MMF for a simple two pole. If phase as is sinusoidally distributed then the MMF in the gap resulting from current flowing in phase a is

$$F_{as} = \frac{N_s}{2} i_{as} \cos \beta. \quad 0 \leq \beta \leq 2\pi \quad (15.38)$$

where N_s is the effective number of turns and β is the angle measured in the counterclockwise direction from the magnetic axis of phase as . Similarly, if currents flow in phases bs or cs which are spatially displaced from phase as by 120 electrical degrees, then the respective air gap MMFs are:

$$F_{bs} = \frac{N_s}{2} i_{bs} \cos\left(\beta - \frac{2\pi}{3}\right) \quad (15.39)$$

$$F_{cs} = \frac{N_s}{2} i_{cs} \cos\left(\beta + \frac{2\pi}{3}\right) \quad (15.40)$$

As written Eqs. (15.38) to (15.40) are real quantities. They would be more physically insightful if these equations were given spatial properties such that their maximum values were directed along their magnetic axes which are clearly spatially oriented $\pm 120^\circ$ with respect to the magnetic axis of phase as . This can be done by introducing a complex plane in which the unit amplitude operator $\bar{a} = e^{j2\pi/3}$ provides the necessary spatial orientation. Specifically spatial quantities \bar{F}_{bs} and \bar{F}_{cs} can now be defined where

$$\bar{F}_{bs} = \bar{a} F_{bs} = \bar{a} \frac{N_s}{2} i_{bs} \cos\left(\beta - \frac{2\pi}{3}\right) \quad (15.41)$$

$$\bar{F}_{cs} = \bar{a}^{\dagger} F_{cs} = \bar{a}^{\dagger} \frac{N_s}{2} i_{cs} \cos\left(\beta - \frac{2\pi}{3}\right) \quad (15.42)$$

where \dagger denotes the complex conjugate.

The net (total) stator air gap MMF expressed as a space vector is simply the sum of the three components or

$$\bar{F}_{abc s} = F_{as} + \bar{a}F_{bs} + \bar{a}^2F_{cs} \quad (15.43)$$

Introducing the Euler equation

$$e^{j\beta} = \cos\beta + j\sin\beta \quad (15.44)$$

Eq. (15.43) can be manipulated to the form

$$\bar{F}_{abc s} = \left(\frac{3}{2}\right)\left(\frac{N_s}{2}\right)(\bar{i}_{abc s} e^{-j\beta} + \bar{i}_{abc s}^\dagger e^{j\beta}) \quad (15.45)$$

where, if the three phase current sum to zero,

$$\bar{i}_{abc s} = i_{as} + \bar{a}i_{bs} + \bar{a}^2i_{cs} \quad (15.46)$$

$$= i_{as} + j\frac{1}{\sqrt{3}}(i_{bs} - i_{cs}) \quad (15.47)$$

Eq. (15.45) is general in the sense that the three stator currents are arbitrary functions of time (but must sum to zero). Consider now the special case when the currents are balanced and sinusoidal. In this case it can be shown that

$$\bar{i}_{abc s} = Ie^{j\theta} \quad (15.48)$$

and $\bar{i}_{abc s}^\dagger = 0$

where I is the amplitude of each of the phase currents and $\theta = \omega t$. The corresponding MMF is

$$\bar{F}_{abc s} = \left(\frac{3}{2}\right)\left(\frac{N_s}{2}\right)I_s e^{j(\theta - \beta)} \quad (15.49)$$

The stator current $\bar{i}_{abc s}$ in complex form can be clearly visualized as a “vector” having a length I_s making an angle θ with respect to the real axis. On the other hand, the complex MMF quantity $\bar{F}_{abc s}$ is not strictly a vector since it has spatial as well as temporal attributes. In particular $\bar{F}_{abc s}$ varies as a sinusoidal function of the spatial variable β . However at a particular time instant $t = \theta/\omega$ the maximum positive value of the MMF is, from (15.49), clearly located spatially at $\beta = \theta$. Hence, the *temporal (time) position of the current vector also locates the instantaneous spatial position of the corresponding MMF amplitude*. This basic tenet is essential for the understanding of AC motor control.

It can be further shown that the temporal position of the air gap flux linkage can be related to the position of the corresponding flux density by

$$\bar{B}_{abc(ag)} = \frac{1}{\left(\frac{2}{\pi} \tau_p l_e N_s\right)} \lambda_{(ag)} e^{j(\theta - \gamma)} \quad (15.50)$$

where $\lambda_{(ag)}$ is the length of the vector $\bar{\lambda}_{abc(ag)}$. Thus the *location of a flux linkage vector in the complex plane* γ uniquely locates the position of the amplitude of the corresponding flux density along the air gap of the machine. While not strictly correct in terms of having spatial properties along the air gap, the flux linkage corresponding to leakage flux is also given an spatial interpretation in which case, for example, the total rotor flux linkage can be defined as

$$\bar{\lambda}_{abcr} = L_2 \bar{i}_{abcr} + L_m (\bar{i}_{abcs} + \bar{i}_{abcr}) \quad (15.51)$$

where \bar{i}_{abcs} and \bar{i}_{abcr} are the three phase motor stator and rotor currents treated a complex quantities as in Eq. (15.46).

It should now be clear that while torque production in an AC machine is physically produced by the interaction (alignment) of the stator MMF relative to the air gap flux density, it is completely equivalent to view torque production as the interaction (alignment) of the stator current vector with respect to the air gap flux linkage vector. This is the principle of control methods which concentrates on instantaneous positioning of the stator current vector with respect to a presumed positioning of the rotor flux vector. The fact that these temporal based vectors produce spatial positioning of field quantities which are in simple proportion to these vectors has prompted the use of the term *space vectors* for such quantities and the control method termed *field orientation*.

15.5.2 The d–q Equations of a Squirrel Cage Induction Motor

Motion control system requirements are typically realized by employing torque control concepts in the induction machine which are patterned after DC machine torque control. The action of the commutator of a DC machine in holding a fixed, orthogonal spatial angle between the field flux density and the armature MMF is emulated in induction machines by orienting the stator current with respect to the rotor flux linkages (i.e the stator MMF with respect to the rotor flux density as explained above) so as to attain independently con-

trolled flux and torque. Such controllers are called *field-oriented controllers* and require independent control of both magnitude and phase of the AC quantities and are, therefore, also referred to as *vector controllers*. The terms “field orientation” and “vector control” are today used virtually interchangeably.

It can be noted from (15.47) that the current vector describing behavior of the three phase currents reduces to a complex two phase quantity if one defines,

$$\dot{i}_{qs}^s = i_{as} \quad (15.52)$$

and

$$\dot{i}_{ds}^s = \frac{1}{\sqrt{3}}(i_{cs} - i_{bs}) \quad (15.53)$$

The symbols d - q and the polarity of the current i_{ds}^s is specifically selected to be consistent with conventions set up for the synchronous machine. The superscript “s” is used to indicate that the reference axes used to define the d - q currents are “stationary”, i.e. non-rotating or fixed to the stator. The differential equations of the squirrel cage machine employing the complex d - q notation of Eqs. (15.47),(15.52) and (15.53) are [22],

$$\bar{v}_{qds}^s = r_1 \bar{i}_{qds}^s + p\lambda_{qds}^s \quad (15.54)$$

$$0 = r_2 \bar{i}_{qdr}^s + p\bar{\lambda}_{qdr}^s - j\omega_r \bar{\lambda}_{qdr}^s \quad (15.55)$$

$$T_e = \frac{3}{2} \cdot \frac{P}{2} \cdot \frac{L_m}{L_r} (\lambda_{dr}^s i_{qs}^s - \lambda_{qr}^s i_{ds}^s) \quad (15.56)$$

A basic understanding of the decoupled flux and torque control resulting from field orientation can now be attained from the d - q axis model of an induction machine with the reference axes rotating at synchronous speed ω_e [22].

$$\bar{v}_{qds}^e = r_1 \bar{i}_{qds}^e + p\lambda_{qds}^e + j\omega_e \bar{\lambda}_{qds}^e \quad (15.57)$$

$$0 = r_2 \bar{i}_{qdr}^e + p\bar{\lambda}_{qdr}^e + j(\omega_e - \omega_r) \bar{\lambda}_{qdr}^e \quad (15.58)$$

$$T_e = \frac{3}{2} \cdot \frac{P}{2} \cdot \frac{L_m}{L_r} (\lambda_{dr}^e i_{qs}^e - \lambda_{qr}^e i_{ds}^e) \quad (15.59)$$

where

$$\bar{v}_{qds}^e = v_{qs}^e - jv_{ds}^e, \quad \bar{i}_{qds}^e = i_{qs}^e - ji_{ds}^e, \quad \bar{i}_{qdr}^e = i_{qr}^e - ji_{dr}^e \quad (15.60)$$

$$\bar{\lambda}_{qds}^e = \lambda_{qs}^e - j\lambda_{ds}^e = L_1 \bar{i}_{qds}^e + L_m (\bar{i}_{qds}^e + \bar{i}_{qdr}^e) \quad (15.61)$$

$$\bar{\lambda}_{qdr}^e = \lambda_{qr}^e - j\lambda_{dr}^e = L_2 \bar{i}_{qdr}^e + L_m (\bar{i}_{qds}^e + \bar{i}_{qdr}^e) \quad (15.62)$$

and $L_r = L_2 + L_m$, and r_1, r_2, L_1, L_2 and L_m are the per-phase stator and rotor resistance, leakage inductances and magnetizing inductance respectively for a star connected machine. Also P denotes the number of poles and p is the time derivative operator d/dt . In these equations the superscript “ e ” is intended to indicate that the reference axes are rotating with the *electrical* frequency. The effect of iron loss is typically neglected in these equations but can be easily incorporated if necessary.

Since the d - q representation may be unfamiliar to the reader it is instructive to consider the form of these equations when steady state is reached. From Eq. (15.48) it is apparent that when the phase currents are balanced, the space vector associated with stator current \bar{i}_{qds}^e rotates with constant angular velocity ω with a constant amplitude I_s . If this same vector is portrayed in a reference which rotates with the vector itself, the synchronous frame representation is simply a complex constant. Similar statements apply for the stator voltage and rotor current vectors and thus for the flux linkage vectors. Since all of the vectors are constant in the steady state the terms of Eqs. (15.57) and (15.58) are zero. These equations become, for the steady state

$$\bar{V}_{qds} = r_1 \bar{I}_{qds} + j\omega_e \bar{\Lambda}_{qds} \quad (15.63)$$

$$0 = r_2 \bar{I}_{qdr} + j(\omega_e - \omega_r) \bar{\Lambda}_{qdr} \quad (15.64)$$

where the use of capitals denote steady state values (constants). Utilizing Eqs. (15.60) and (15.61) it is not difficult to show that these two equations can be manipulated to the form,

$$\bar{V}_{qds}^e = r_1 \bar{I}_{qds}^e + j\omega_e [L_1 \bar{I}_{qds}^e + L_m (\bar{I}_{qds}^e + \bar{I}_{qdr}^e)] \quad (15.65)$$

$$0 = \frac{\omega_e r_2}{(\omega_e - \omega_r)} \bar{I}_{qdr}^e + j\omega_e [L_2 \bar{I}_{qdr}^e + L_m (\bar{I}_{qds}^e + \bar{I}_{qdr}^e)] \quad (15.66)$$

which are nothing more than the conventional per phase phasor equations for an induction motor in the steady state wherein the variables are expressed in terms of their peak rather than rms values. Thus the induction motor d - q equa-

tions in the synchronous frame are simply an extension of the conventional phasor equations to account for transient conditions.

15.5.3 The Field Orientation Principle

The field orientation concept implies that the current components supplied to the machine should be oriented in such a manner as to isolate the component of stator current magnetizing the machine (flux component) from the torque producing component. This can be accomplished by choosing the reference frame speed ω_e to be the instantaneous speed of the rotor flux linkage vector $\bar{\lambda}_{qdr}^e$ and locking its phase such that the rotor flux is entirely in the d -axis (now equivalent to the flux or magnetizing axis), resulting in the mathematical constraint

$$\lambda_{qr}^e = 0 \quad (15.67)$$

Assuming the machine is supplied from a current regulated source so the stator equations can be omitted, the d - q equations in a rotor flux-oriented (field-oriented) frame become

$$0 = r_2 i_{qr}^e - (\omega_e - \omega_r) \lambda_{dr}^e \quad (15.68)$$

$$0 = r_2 i_{dr}^e + p \lambda_{dr}^e \quad (15.69)$$

$$\lambda_{dr}^e = L_m i_{ds}^e + L_r i_{dr}^e \quad (15.70)$$

$$\lambda_{qr}^e = 0 = L_m i_{qs}^e + L_r i_{qr}^e \quad (15.71)$$

$$T_e = \frac{3}{2} \cdot \frac{P}{2} \cdot \frac{L_m}{L_r} \lambda_{dr}^e i_{qs}^e \quad (15.72)$$

The torque equation (15.72) clearly shows the desirable torque control property of a DC machine, that of providing a torque proportional to the armature current component i_{qs}^e . A direct (ampere-turn or MMF) equilibrium relation between the torque command current i_{qs}^e and the rotor current i_{qr}^e follows immediately from (15.71)

$$i_{qr}^e = -\frac{L_m}{L_r} i_{qs}^e \quad (15.73)$$

so that this component of stator current does not contribute to the rotor flux component producing torque, i.e the flux linkage λ_{dr}^e .

Combining (15.68) and (15.73) yields another algebraic constraint which is commonly called the *slip relation*

$$s\omega_e = -r_2 \frac{L_m i_{qs}^e}{L_r \lambda_{dr}^e} \quad (15.74)$$

which must always be satisfied by means of control if the constraint of (15.71) is to be satisfied.

Equation (15.69) shows that in the steady-state when λ_{dr}^e is constant, the rotor current component i_{dr}^e is zero. However, whenever the flux changes, i_{dr}^e is not zero but is given by

$$i_{dr}^e = \frac{1}{r_2} p \lambda_{dr}^e \quad (15.75)$$

Combining (15.75) and (15.70) to eliminate i_{dr}^e yields the equation relating i_{ds}^e and λ_{dr}^e (flux producing component of stator current and resulting rotor flux)

$$\lambda_{dr}^e = \frac{r_2 L_m}{r_2 + L_r p} i_{ds}^e \quad (15.76)$$

where the operator p can now be interpreted as equivalent to the Laplace operator s .

The close parallel to the DC machine now becomes clear. Equation (15.72) emphasizes this correspondence in terms of torque production. The relation between the flux command current i_{ds}^e and the rotor flux λ_{dr}^e is a first-order linear transfer function with a time constant T_r , where

$$T_r = \frac{L_r}{r_2} \quad (15.77)$$

This resistance corresponds to the open circuit field winding time constant of a DC machine, where the time constant T_r is that associated with the field winding time constant. The slip relation expresses the slip frequency which is inherently associated with the division of the input stator current into the desired flux and torque components. It is useful to also note that, in contrast to a DC motor, the ampere turn balance expressed in Eq. (15.73) implies there is no “armature reaction” in a field-oriented controlled induction machine. The cross-magnetizing component i_{qs}^e that produces the torque is cancelled by i_{qr}^e , and thus there is no effect on rotor flux even under saturated conditions.

Field orientation with respect to fluxes other than the rotor flux is also possible [23] with the stator and air gap fluxes being the most important alternatives. Only the rotor flux yields complete decoupling, however, for some purposes (wide range field weakening operation for example) the advantages of choosing stator flux orientation can outweigh the lack of complete decoupling [24].

15.5.4 Direct Field Orientation

In direct field orientation the position of the flux to which orientation is desired is directly measured using sensing coils or estimated from terminal measurements. Since it is not possible to directly sense the rotor flux, a rotor flux-oriented system must employ some type of computation to obtain the desired information from a directly sensed signal. Figure 15.22 illustrates the nature of these computations for terminal voltage and current sensing; the most frequently used technique for direct field orientation.

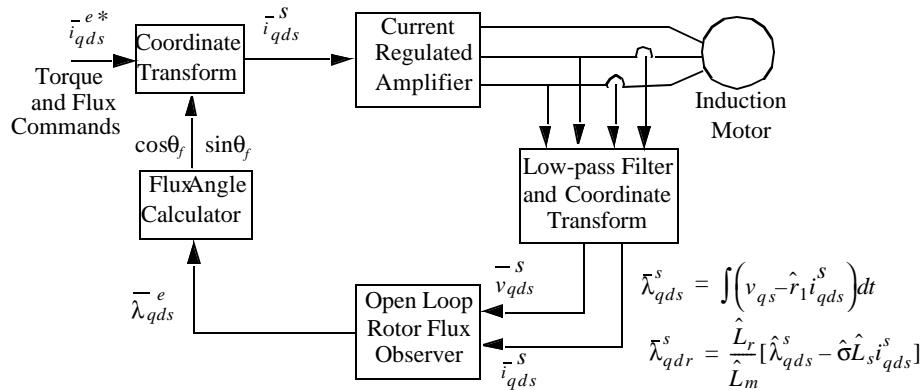


Figure 15.22 Direct field orientation with rotor field angle θ_f determined from terminal voltage and current, “ \wedge ” denotes estimate of a motor parameter, “ $*$ ” a commanded quantity, $\sigma = 1 - L_m^2/(L_r L_s)$

In cases where flux amplitude information is available, a flux regulator can be employed to improve the flux response. A variety of flux observers can be employed to obtain improved response and less sensitivity to machine parameters. Some of these are discussed in a later section. A major problem with most direct orientation schemes is their inherent problems at very low speeds where

the machine T_r drops are dominant and/or the required integration of signals becomes problematic.

15.5.5 Indirect (Feedforward) Field Orientation

An alternative to direct sensing of flux position is to employ the slip relation, Eq. (15.74), to estimate the flux position relative to the rotor. Figure 15.23 illustrates this concept and shows how the rotor flux position can be obtained by adding the integral of the slip frequency calculated from the flux and torque commands to the sensed rotor position to produce an angular estimate of the rotor flux position. In the steady-state this approach corresponds to setting the slip to the specific value which correctly divides the input stator current into the desired magnetizing (flux producing) and secondary (torque producing) currents. Indirect field orientation does not have inherent low-speed problems and is thus preferred in most systems that must operate near zero speed.

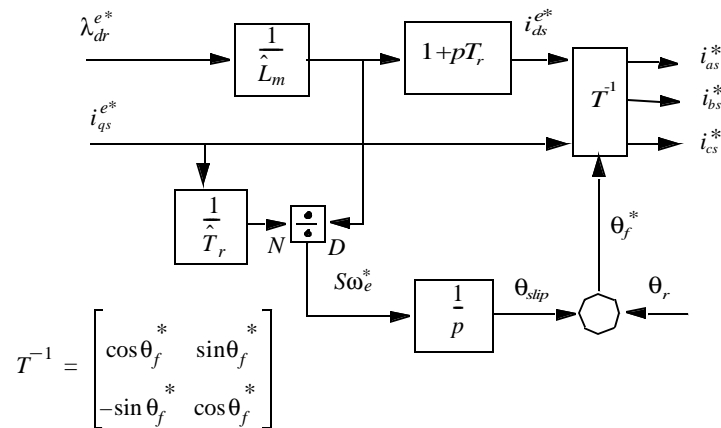


Figure 15.23 Indirect field orientation controller using rotor flux and torque producing current commands

15.5.6 Influence of Parameter Errors

Since knowledge of the machine parameters are a part of the feedback or feed-forward controllers, both basic types of field orientation have some sensitivity to machine parameters and provide non-ideal torque control characteristics when control parameters differ from the actual machine parameters. In general both steady-state torque control and dynamic response differ from the ideal instantaneous torque control achieved by a correctly tuned controller.

The major problem in the use of indirect control is the required knowledge of the rotor open circuit time constant T_r , which is sensitive to both temperature and flux level [25]. When this parameter is incorrect in the controller the calculated slip frequency is incorrect and the flux angle is no longer appropriate for field orientation. This results in an instantaneous error in both flux and torque which can be shown to excite a second order transient characterized by eigenvalues having a real part equal to $-1/T_r$ and an oscillation frequency related to the (incorrect) commanded slip frequency. Since T_r is an open circuit time constant and therefore rather large, these oscillations can be poorly damped. There is also a steady-state torque amplitude error since the steady-state slip is also incorrect. Steady state slip errors also cause additional motor heating and reduced efficiency.

Direct field orientation systems are generally sensitive to stator resistance and total leakage inductance, but the various systems have individual detuning properties. Typically, parameter sensitivity is less than in indirect control, especially when a flux regulator is employed. In all cases, both direct and indirect, parameter sensitivity depends on the ratio $\sigma L_s/r_1$ with larger values giving greater sensitivity. In the steady-state the quantity determines the location of the peak torque and thus the shape of the torque versus slip frequency characteristic. Thus, large, high efficiency machines tend to have high sensitivity to parameter errors, and field weakened operation further aggravates this sensitivity.

15.5.7 Current Regulation

It has gradually been recognized that field oriented control allows speed loop bandwidths far exceeding that of the DC motor (100 Hz or more) making induction motor servos the device favored for demanding applications. However such a bandwidth can only be achieved with careful tuning of the current regulator which serves to overcome the stator transient time constant. Current regulators remain a rich area of research. However, the present methods can be categorized generally as follows:

- Sine-Triangle Current Regulation
- Hysteresis Current Regulation
- Predictive (dead-beat) Current Regulation.

The three types of regulators are illustrated in Figure 15.24.

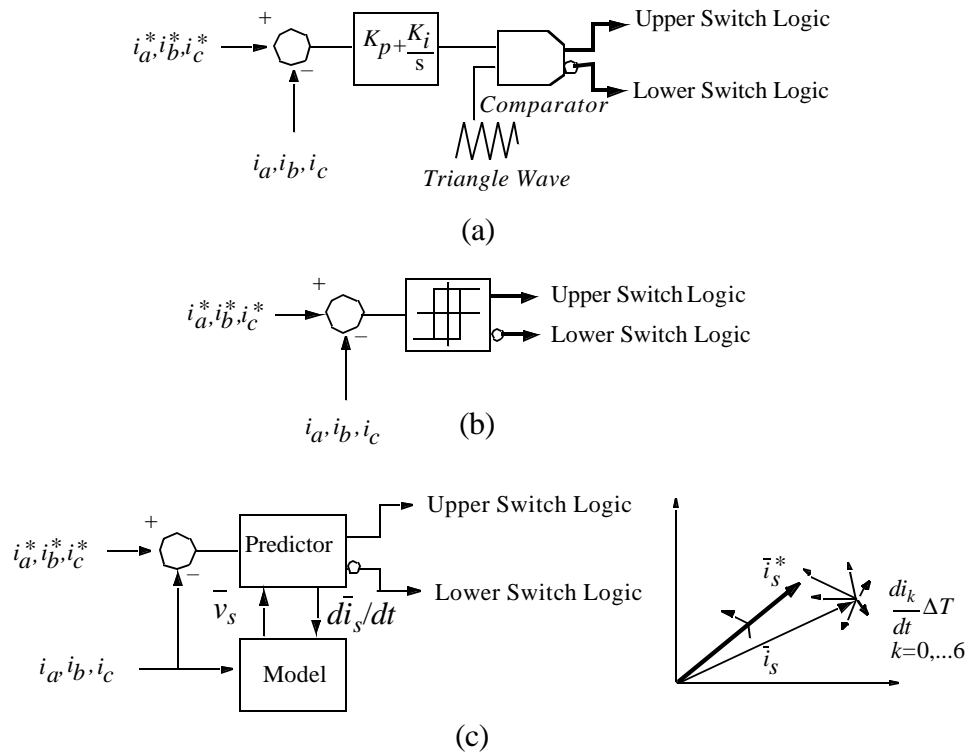


Figure 15.24 Basic current regulation schemes, (a) three phase sine-triangle comparison (b) three phase hysteresis control (c) predictive regulation

The sine triangle intersection method uses the same basic principles as sine-triangle pulse width modulation except that the input command to the comparator is the error between a desired current value and the actual instantaneous value. Hence, the controller attempts to control the input current error to zero. The current error in Figure 15.24(a) can be interpreted as the equivalent to an instantaneous voltage command V_1^* of zero in Figure 15.14. An advantage of this controller is that the switching frequency is set by the triangle wave frequency so that the harmonic structure is not appreciably altered when compared with voltage PWM. Care must be taken however not to introduce excessive proportional gain or added intersections command and triangle wave could occur as a result of the harmonics introduced by the current feedback. Excessive integrator gain on the other hand can cause oscillatory behavior. Because of the phase shift introduced by the integrator, the current error of this regulator can not be reduced to zero if the input command is sinusoidal (as is

usually the case). Hence, the regulation is usually accomplished in the synchronous frame, operating on current commands which becomes constant in the steady state (see Section 15.5.2) [26].

The hysteresis regulator of Figure 15.24(b) produces switching whenever the sign of the current error plus the hysteresis band changes polarity. The proper setting of the hysteresis band is critical for this type of controller since the band essentially sets the switching frequency. However, the frequency of switching is not constant because the voltage producing a current change is equal to the difference between the applied inverter voltage and the internal EMF of the machine. Since the EMF varies sinusoidally throughout a cycle, the pulse (switching) frequency varies throughout the cycle. Since the switching frequency becomes a variable dependant upon the instantaneous value of back-EMF, the spectrum produced by the switching events are spread over a continuous band of frequency and becomes difficult to predict. Thus, computation of motor losses produced by this type of input becomes very difficult. Means for reducing the switching frequency variation have been reported [28], [29] and work is ongoing.

The third type of current regulator is the predictive regulator of Figure 15.24(c). It can be recalled from Section 15.4.4 that switching of a three phase inverter is characterized by only 8 state including two with zero voltage output. Hence, only 7 unique switching states exist as shown in Figure 15.17. If the future trajectory of the current is calculated just before each switching event for all seven unique switch states, then the trajectory which directs the current space vector in the best direction for tracking the commanded current can be determined or predicted. Clearly the accuracy of the method is critically dependant upon the motor model which is used to predict the current trajectory. Many variations on this theme exist with Refs. [29] and [30] being a good starting point.

15.5.8 “Sensorless” Speed Control

As AC motor drives have gradually matured, the cost and unreliability of the speed/position encoder required for field oriented control has gradually been recognized. Beginning with Joetten and Maeder [31], work has continued on a myriad of alternatives to eliminate the speed/position sensor, many of which have appeared in manufacturer’s equipment. In reality, of course, these “sensorless” methods refer only to the fact that speed is not explicitly mea-

sured but, rather, is inferred from electrical measurements and the machine model.

As an introduction to the approach, the d -axis components of the squirrel cage induction machine in a fixed, non-rotating frame “ s ” can be written, from Section 15.5.2,

$$v_{ds}^s = r_1 i_{ds}^s + \frac{d\lambda_{ds}^s}{dt} \quad (15.78)$$

$$0 = r_2 i_{dr}^s + \omega_r \lambda_{qr}^s + \frac{d\lambda_{dr}^s}{dt} \quad (15.79)$$

$$\lambda_{ds}^s = L_s i_{ds}^s + L_m i_{dr}^s \quad (15.80)$$

$$\lambda_{dr}^s = L_r i_{dr}^s + L_m i_{ds}^s \quad (15.81)$$

where $L_s = L_1 + L_m$ and $L_r = L_2 + L_m$. Solving Eq. (15.81) for i_{dr}^s and substituting the result into Eq. (15.80),

$$\lambda_{ds}^s = \frac{L_m}{L_r} \lambda_{dr}^s + \sigma L_s i_{ds}^s \quad (15.82)$$

where $\sigma = 1 - L_m^2 / (L_s L_r)$, or

$$\lambda_{dr}^s = \frac{L_r}{L_m} \lambda_{ds}^s - \frac{\sigma L_r L_s}{L_m} i_{ds}^s \quad (15.83)$$

The back emf of the d -axis rotor circuit is therefore

$$e_{dr}^s = \frac{d\lambda_{dr}^s}{dt} = \frac{L_r}{L_m} \frac{d\lambda_{ds}^s}{dt} - \sigma \frac{L_s L_r}{L_m} \frac{di_{ds}^s}{dt} \quad (15.84)$$

or, from Eq. (15.78)

$$e_{dr}^s = \frac{L_r}{L_m} (v_{ds}^s - r_1 i_{ds}^s) - \sigma \frac{L_s L_r}{L_m} \frac{di_{ds}^s}{dt} \quad (15.85)$$

In the same manner, for the q -axis emf

$$\lambda_{qr}^s = \frac{L_r}{L_m} \lambda_{qs}^s - \frac{\sigma L_r L_s}{L_m} i_{qs}^s \quad (15.86)$$

$$e_{qr}^s = \frac{L_r}{L_m} (v_{qs}^s - r_1 i_{qs}^s) - \sigma \frac{L_s L_r}{L_m} \frac{di_{qs}^s}{dt} \quad (15.87)$$

Finally, from Eq. (15.79), the rotor speed can now be expressed as

$$\omega_r = \frac{1}{\lambda_{qr}^s} \left[r_2 \left(\frac{\lambda_{dr}^s}{L_r} - \frac{L_m}{L_r} i_{ds}^s \right) - e_{dr}^s \right] \quad (15.88)$$

where, λ_{qr}^s is obtained from Eq. (15.86), and e_{dr}^s from Eq. (15.85). A block diagram of the complete speed sensor, developed previously in [32], is shown in Figure 15.25. Clearly, perfect knowledge of all of the machine parameters are needed to implement the approach which is rarely the case. However a reasonable estimate of the parameters provide a speed estimate which is adequate for moderate response speed control which does not include lengthy operation near zero speed. A multitude of variations of this principle have appeared in

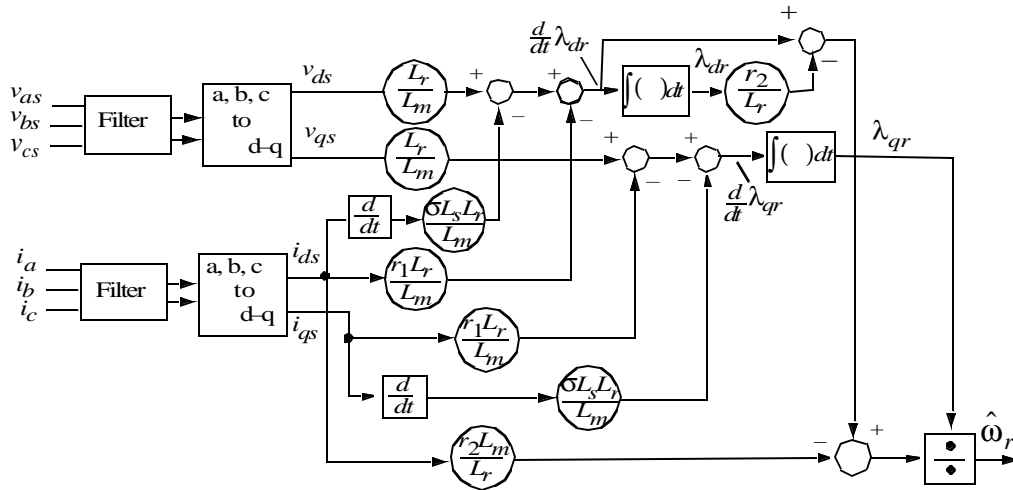


Figure 15.25 “Sensorless” sensing of rotor speed; mechanical speed in rad./sec. $\omega_{rm} = \omega_r/(P/2)$ where P is the number of poles

the literature which is nicely summarized in Ref. [32].

15.6 Induction Motor Observer

After 50 years of AC drive development the design of a sensorless induction motor drive is still an engineering challenge. The basic problem is the need for speed estimation which becomes especially difficult at low speed and under a light load condition. The majority of speed identification methods rely on an

approximate fundamental component model of the machine. The use of the stator equation, particularly the integration of the stator voltage vector, is common for all methods. Its solution is fairly accurate when the switched stator voltage waveform is measured at high bandwidth and when the parameters that determine the contributions of the resistive and the leakage voltage components are well known. As the influence of these parameters dominates the estimation at low speed, the steady state accuracy of speed sensorless operation tends to be poor in during low or zero speeds.

One promising approach to solving this barrier is the *sliding mode* approach to rotor flux and speed estimation of an induction machine. The sliding mode method is a non-linear method for feedback control, state estimation and parameter identification [33]. The property of the sliding mode approach is due to use of straightforward fixed non-linear feedback control functions that operate effectively over a specified magnitude range of system parameter variations and disturbances.

From Eq. (15.84) and (15.85) one can note that the rotor flux is related to the stator voltage by

$$\frac{L_m d\lambda_{dr}^s}{L_r dt} = v_{ds}^s - i_{ds}^s r_1 - \sigma L_s \frac{di_{ds}^s}{dt} \quad (15.89)$$

where the second two terms (Ir and leakage Ldi/dt drop) can be considered as corrections to the major term, the applied d -axis voltage. This equation defines what is called the *voltage model*. A similar equation applies for the q -axis circuit.

Alternatively the d -axis rotor flux can be calculated by combining Eqs. (15.79) and (15.82) whereupon

$$\frac{d\lambda_{dr}^s}{dt} = -\omega_r \lambda_{qr}^s - \frac{r_2}{L_r} \lambda_{dr}^s + r_2 \frac{L_m}{L_r} i_{ds}^s \quad (15.90)$$

In this case the input to the equation is the stator current and thus forms the *current model*. Similar expressions for the q -axis rotor flux components can be readily obtained.

In the interests of compactness it is convenient to cast these equations in complex form, similar to Eqs. (15.54) and (15.55), as

$$\frac{L_m d\bar{\lambda}_{qdr}^s}{L_r dt} = \bar{v}_{qds}^s - \bar{i}_{qds}^s r_1 - \sigma L_s \frac{d\bar{i}_{qds}^s}{dt} \quad (\text{voltage model})(15.91)$$

and

$$\frac{d\bar{\lambda}_{qdr}^s}{dt} = \left(j\omega_r - \frac{r_2}{L_r} \right) \bar{\lambda}_{qdr}^s + r_2 \frac{L_m}{L_r} \bar{i}_{qds}^s \quad (\text{current model})(15.92)$$

The most significant limitation of the rotor flux observer based on voltage model is that it does not function at zero speed. At zero speed and low speed the amplitude of the electromotive force is too small to accurately and reliably determine the rotor flux angle necessary for both field orientation and speed estimation. At low speed the flux estimation given by voltage model deteriorates owing to the effect of an inaccurate value of the stator resistance r_1 , which causes a slight deviation of the rotor flux space vector. The current model requires information about speed, so in a speed sensorless control one needs to estimate both the rotor flux and mechanical speed.

To achieve a current based observer suitable for a sensorless drive, the observer control input should be a known function of motor speed so that, after establishing a sliding mode in a torque tracking loop, the speed can be determined as a unique solution [34]. Combining the voltage and current model,

$$\frac{d\bar{i}_{qds}^s}{dt} = \frac{1}{\sigma L_s} \left[\bar{v}_{qds}^s - r_1 \bar{i}_{qds}^s - \frac{L_m}{L_r} \left(\bar{e}_{qdr}^s + r_2 \frac{L_m}{L_r} \bar{i}_{qds}^s \right) \right] \quad (15.93)$$

where, the emf

$$\bar{e}_{qdr}^s = \left(j\omega_r - \frac{r_2}{L_r} \right) \bar{\lambda}_{qdr}^s \quad (15.94)$$

A current estimation error can be defined as

$$\frac{d\bar{\epsilon}_i}{dt} = \frac{d(\bar{i}_{qds}^s - \hat{i}_{qds}^s)}{dt} = \frac{1}{\hat{\sigma} L_s} \left\{ \frac{L_m}{L_r} (\bar{e}_{qdr}^s - \hat{\bar{e}}_{qdr}^s) - \left[\hat{r}_1 + \hat{r}_r \left(\frac{\hat{L}_m}{\hat{L}_r} \right)^2 \right] \cdot \bar{\epsilon}_i \right\} \quad (15.95)$$

and the carat “^” again denotes an estimate.

If the derivative in (15.95) is written in discretized form,

$$\frac{d\bar{\epsilon}_i}{dt} = \frac{1}{T} [\bar{\epsilon}_i(k) - \bar{\epsilon}_i(k-1)] \quad (15.96)$$

Equation (15.95) can be rewritten as

$$\bar{\epsilon}_i(k) - \bar{\epsilon}_i(k-1) = \frac{T}{\hat{\sigma} \hat{L}_s} \left\{ \frac{\hat{L}_m}{\hat{L}_r} [\bar{e}_{qdr}^s(k) - \hat{e}_{qdr}^s(k)] - \left[\hat{r}_1 + \hat{r}_2 \left(\frac{\hat{L}_m}{\hat{L}_r} \right)^2 \right] \cdot \bar{\epsilon}_i \right\} \quad (15.97)$$

which can be rearranged to the form

$$\bar{e}_{qdr}^s(k) - \hat{e}_{qdr}^s(k) = \frac{\hat{\sigma} \hat{L}_s \hat{L}_m}{T \hat{L}_r} \left\{ \left[1 + \frac{T}{\hat{\sigma} \hat{L}_s} \left[\hat{r}_1 + \hat{r}_2 \left(\frac{\hat{L}_m}{\hat{L}_r} \right)^2 \right] \right] \bar{\epsilon}_i(k) - \bar{\epsilon}_i(k-1) \right\} \quad (15.98)$$

Upon examining Eq. (15.98) it is clear that if the current error $\bar{\epsilon}_i(k)$ is driven to zero then the error in the estimate of the emf is driven to zero. This observation can be employed to implement a controller which, by utilization of a current regulated PWM algorithm (Figure 15.24) the current error can be driven to zero. Hence, an estimate of the rotor back emf can be obtained.

A new updated value of emf at time step k based on the previous value at time step $k-1$ plus the current estimation error can now be expressed as

$$\hat{e}_{qdr}(k) = \bar{e}_{qdr}(k-1) + \frac{\hat{\sigma} \hat{L}_s \hat{L}_r}{T \hat{L}_m} [(1 + TD_i) \bar{\epsilon}_i(k) - \bar{\epsilon}_i(k-1)] \quad (15.99)$$

where T is the length of the time step (sampling time) and $D_i = (r_1 + r_2(L_m/L_r)^2)/(\sigma L_s)$. The process of zeroing the error utilizing current regulated PWM is the essence of *sliding mode control*.

A rotor flux observer can now be selected by utilizing Eq. (15.94), whereupon, solving for the flux linkage

$$\bar{\lambda}_{qdr}^s = - \frac{\left(j\omega_r + \frac{r_2}{L_r} \right)}{\omega_r^2 + \left(\frac{r_2}{L_r} \right)^2} \bar{e}_{qdr}^s \quad (15.100)$$

The speed estimate needed in Eq. (15.100) can be obtained from Figure 15.25. A block diagram of the rotor flux algorithm is given in Figure 15.26. By manipulation of the d - q machine equations other expressions for rotor linkage and rotor speed are possible. For example one could use a simple integration of Eq. (15.91), the voltage model, which performs well for speeds sufficiently far from zero or (15.92), the current model, which is frequently used for low

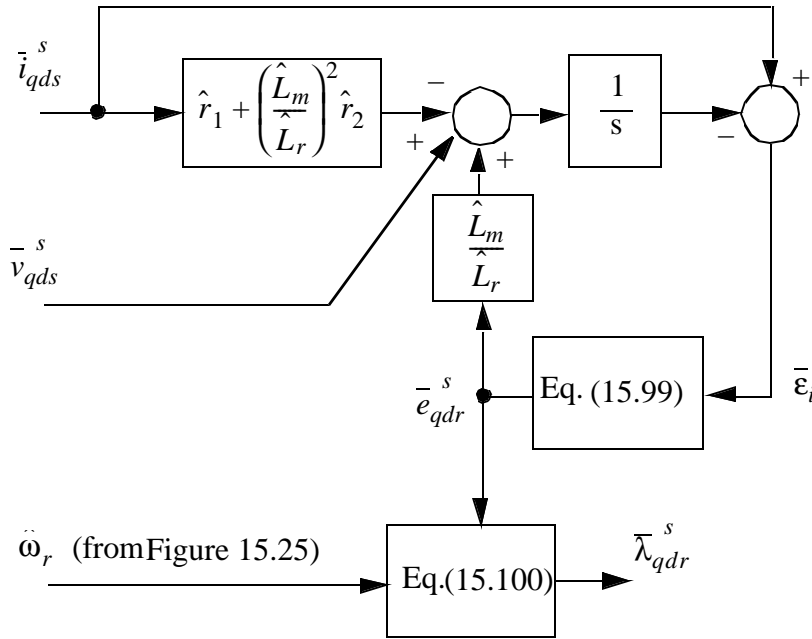


Figure 15.26 Closed loop rotor flux observer

speeds. The reader is referred to the literature [32]–[34] for further information.

15.7 Permanent Magnet AC Machine Control

15.7.1 Machine Characteristics

In contrast to induction machines which are overwhelmingly of the squirrel cage construction, permanent magnet AC (PMAC) machines have been realized in a variety of practical implementations depending upon stator winding pattern, magnet disposition, air gap flux direction (radial, axial or a combination – transverse flux) and presence or absence of a rotor cage. However, two broad categories can be identified 1) trapezoidal EMF machines and 2) sinusoidal EMF machines. The trapezoidal EMF machine is equipped with windings concentrated into only one or at most a few full pitch slots per pole. The magnet disposition of these machines are usually located on the rotor surface and generate a trapezoidal or rectangular EMF in the stator phase windings. The span of the magnets are chosen so as to produce a 120° quasi-rectangular

waveform as shown in Figure 15.27. Since the EMF is rectangular, the optimal stator current waveform is also quasi-rectangular. Rectangular currents are easily obtained by using only a single DC link current sensor and a relatively crude position sensor which requires only a 6P pulses per revolution. However, these machine are plagued with torque pulsation issues which are very complicated due to the effects of armature reaction and are slowly being phased out in favor of sinusoidal EMF machines.

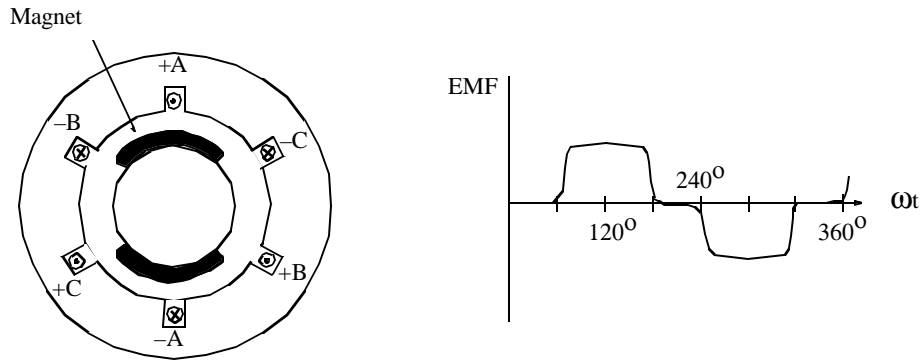


Figure 15.27 Rectangular EMF PM machine utilizing surface magnets

While the stator windings of trapezoidal PMAC machines are concentrated into narrow phase belts, the windings of a sinusoidal machine are typically distributed over multiple slots in order to approximate a sinusoidal distribution. Whereas trapezoidal excitation strongly favors PMAC machines with non-salient rotor designs (surface magnets) so that the phase inductances remain constant as the rotor rotates so as to minimize the effects of armature reaction. In contrast, PMAC machines with salient rotor poles can offer useful performance characteristics when excited with sinusoidal EMF, providing flexibility for adopting a variety of rotor geometries including a variety of inset or buried magnet as alternatives to the baseline surface magnet design as shown in Figure 15.28.

The most convenient manner of analyzing a sinusoidal EMF PMAC machine again uses instantaneous current, voltage, and flux linkage space vectors in a reference frame fixed to the rotor flux presented in Section 15.5.2. In this case the reference frame rotates synchronously with the applied stator field so that the rotor speed in electrical radians per second $\omega_r = \omega_e$. Referring to Eqs. (15.57) to (15.62), these equations can be adapted to characterize a

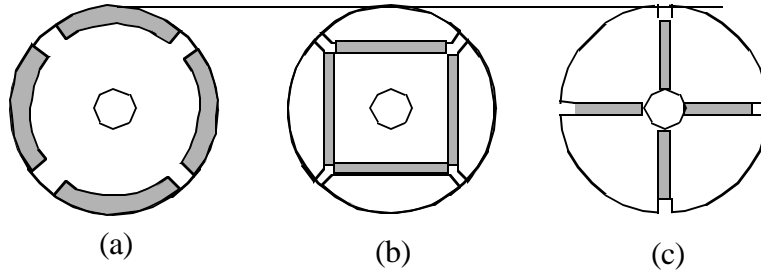


Figure 15.28 Rotor configurations for four pole PMAC machines, (a) inset, (b) interior radial flux and (c) interior circumferential flux magnet orientation

PMAC machine by assuming that the flux produced by the d-axis rotor current is constant. That is, an equivalent permanent magnet field is modeled when

$$L_m i_{dr} = \lambda_m = \text{constant}, \quad L_m i_{qr} = 0 \quad (15.101)$$

Since no time varying currents flow in the rotor, the rotor equation, Eq. (15.58), is not necessary when the rotor does not have a starting cage as is usually the case in a drive application. Combining Eqs. (15.57), (15.61) and (15.101) and separating the complex stator equation into its two components becomes, in scalar form, neglecting iron loss

$$v_{qs}^e = r_1 i_{qs}^e + p(L_1 + L_m) i_{qs}^e + \omega_e (L_1 + L_m) i_{ds}^e + \omega_e \lambda_m \quad (15.102)$$

$$v_{ds}^e = r_1 i_{ds}^e + p(L_1 + L_m) i_{ds}^e - \omega_e (L_1 + L_m) i_{qs}^e \quad (15.103)$$

In cases where the magnets are buried below the rotor surface as in Figure 15.28, the air gap inductances of the two axes must be modified to account for the effect of saliency. With this modification, the equations for a buried magnet machine in the steady state, wherein the $p = d/dt$ terms are set to zero, become

$$V_{qs}^e = r_1 I_{qs}^e + \omega_e (L_1 + L_{mq}) I_{ds}^e + \omega_e \Lambda_m \quad (15.104)$$

$$V_{ds}^e = r_1 I_{ds}^e - \omega_e (L_1 + L_{mq}) I_{qs}^e \quad (15.105)$$

Capital letters are used here to denote steady state conditions. As demonstrated previously, the space vector equations and phasor equations are identical in the steady-state except that space vector representation is usually interpreted in terms of peak values whereas the phasor form is interpreted in terms of rms quantities. A plot of the basic space vector (phasor) relationships for the sinu-

sinoidal EMF PMAC machine is shown in Figure 15.29. The use of the superscript “*e*” has been dropped for simplicity.

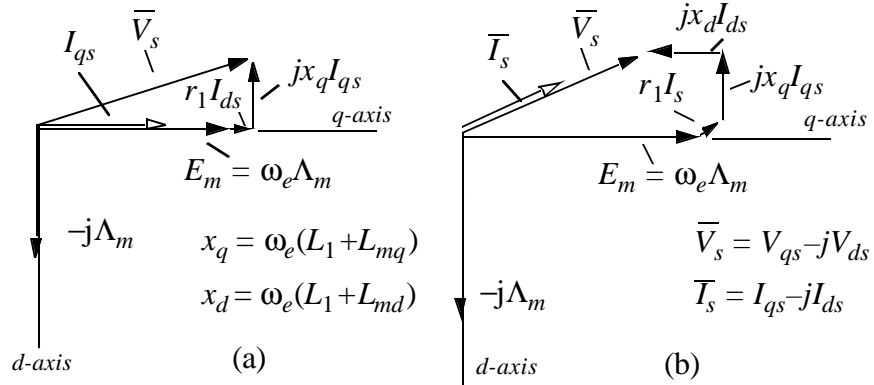


Figure 15.29 Basic steady-state relationships for sinusoidal PMAC machine in synchronously rotating reference frame using *d*-axis alignment with rotor magnet flux linkage $\bar{\lambda}_m$, (a) maximum torque per ampere, (b) unity power factor

As indicated in Figure 15.29, the direct or *d*-axis has been aligned with the permanent magnet flux linkage vector $\bar{\lambda}_m$, so that the orthogonal quadrature or *q*-axis is aligned with its time-rate-of change, the resulting back-EMF E_m . The amplitude of the back-EMF phasor E_m can be expressed very simply as

$$E_m = \omega_e \Lambda_m = \frac{P}{2} \omega_{rm} \lambda_m \quad (15.106)$$

where P is the number of pole pairs ω_{rm} is the mechanical speed in rad/s and Λ_m is the magnet flux linkage amplitude. The sinusoidal three-phase current excitation is expressed in Figure 15.29 as an instantaneous current vector \bar{I}_s made up of *d*- and *q*-axis scalar components i_{ds} and i_{qs} , respectively, and the applied stator voltage phasor \bar{V}_s can be similarly depicted.

The value of magnetizing inductances L_{md} will be smaller than L_{mq} in salient-pole PMAC machines using buried or inset magnets since the total magnet thickness appears as an incremental air gap length in the *d*-axis magnetic circuit (i.e., $\mu_r \cong 1$ for ceramic and rare earth magnet materials). Interior PMAC machine designs of the type shown in Figure 15.28 with a single magnet barrier typically provide L_{mq}/L_{md} ratios in the vicinity of 3, while novel laminated designs have been reported with saliency ratios of 7 or higher.

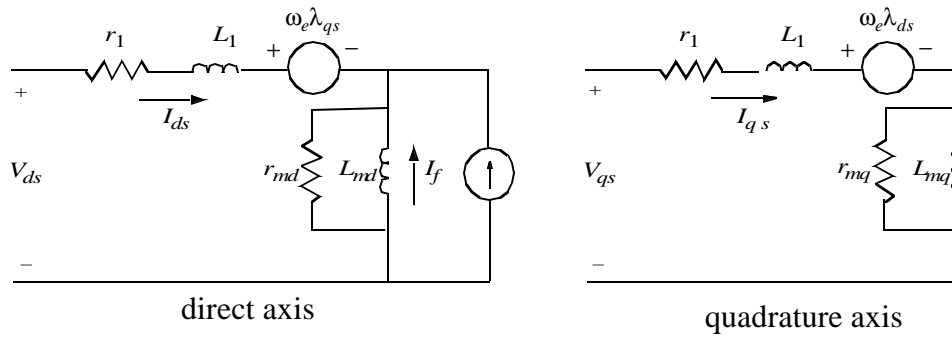


Figure 15.30 Coupled d - q equivalent circuits for a sinusoidal PMAC machine in the synchronously rotating reference frame as defined in Figure 6-22.

This d - q phasor representation leads to the following general expression for the instantaneous torque developed in a sinusoidal PMAC machine,

$$T_e = \frac{3}{2} \cdot \frac{P}{2} \cdot [\lambda_m i_{qs} + (L_d - L_q) i_{ds} i_{qs}] \quad (15.107)$$

where L_d and L_q are the d - and q -axis stator phase inductances, corresponding to $(L_{md} + L_1)$ and $(L_{mq} + L_1)$, respectively, in the Figure 15.30 equivalent circuits. Since L_q is typically larger than L_d in salient pole PMAC machines, it is worth noting that i_{ds} and i_{qs} must have opposite polarities for the second term to contribute a positive torque component. The first “magnet” torque term is independent of i_{ds} but is directly proportional to stator current component i_{qs} which is in phase with the back-EMF E_m . In contrast, the second “reluctance” torque term is proportional to the $i_{ds} \cdot i_{qs}$ current component product and to the difference in the inductance values along the two axes ($L_d - L_q$). This interpretation emphasizes the hybrid nature of the salient pole PMAC machine. Note that the torque is no longer linearly proportional to the stator current amplitude in the presence of magnetic saliency.

15.7.2 Open-Loop V/Hz Control

As discussed briefly in Section 6.1.1, buried-magnet PMAC machines can be designed with an induction motor squirrel cage winding embedded along the surface of the rotor as sketched in Figure 15.31. This hybridization adds a component of asynchronous torque production so that the PMAC machine can be

operated stably from an inverter without position sensors. This simplification makes it practical to use a simple constant volts-per-hertz (V/Hz) control algorithm in much the same manner as for the induction machine. According to this approach, a sinusoidal voltage PWM algorithm is implemented which linearly increases the amplitude of the applied fundamental voltage amplitude in proportion to the speed command to hold the stator magnetic flux approximately constant. Compensation is again required for IR drop and for DC bus voltage changes but, clearly, no compensation is needed for rotor slip.

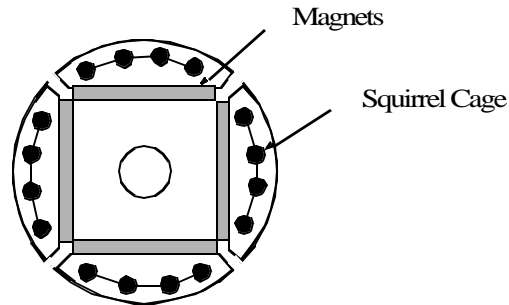


Figure 15.31 Cross section of a four pole PM/induction machine, showing simplified block diagram of open loop volts per-hertz control scheme.

The open loop nature of this control scheme makes it necessary to avoid sudden large changes in the speed command or the applied load to avoid undesired loss of synchronization (pull-out) of the PMAC machine. However, an appealing aspect of this drive configuration is that the same constant volts-per-hertz control approach can be used in many packaged induction motor drives for general-purpose industrial speed control applications. Thus, cage-type PMAC motors can be selected to replace induction motors in some adjustable speed drive applications to improve system operating efficiency without changing the drive control electronics.

15.7.3 High-Performance Closed Loop Control.

In contrast to open loop operation, a rotor position sensor is typically required to achieve high-performance motion control with the sinusoidal EMF PMAC machine. The rotor position feedback needed to continuously perform the self-synchronization function is essentially the same as an induction motor. How-

ever, cogging torque (torque pulsations) due to interaction of the magnets with the stator slot harmonics places a heavier burden on the encoder to smooth out these effects. As a result, an absolute encoder or resolver requiring a high resolution is frequently needed. In addition, in contrast to the induction machine, special provision is frequently needed to provide smooth, controlled starting performance since inappropriate energization at start can produce a brief negative rather than positive rotation.

One baseline approach for implementing this type of high-performance torque control for sinusoidal PMAC machines is shown in Figure 6-25 [36]. According to this approach, the incoming torque command T_e^* (asterisk designates command) is mapped into commands for d - q axis current components i_d^* and i_q^* which are extracted from torque equation, Eq. (15.107). These current commands in the rotor d - q reference frame (essentially DC quantities) are then transformed into the instantaneous sinusoidal current commands for the individual stator phases (i_a^* , i_b^* , and i_c^*) using the rotor angle feedback θ_r , and the inverse vector rotation equations included as part of Figure 15.23.

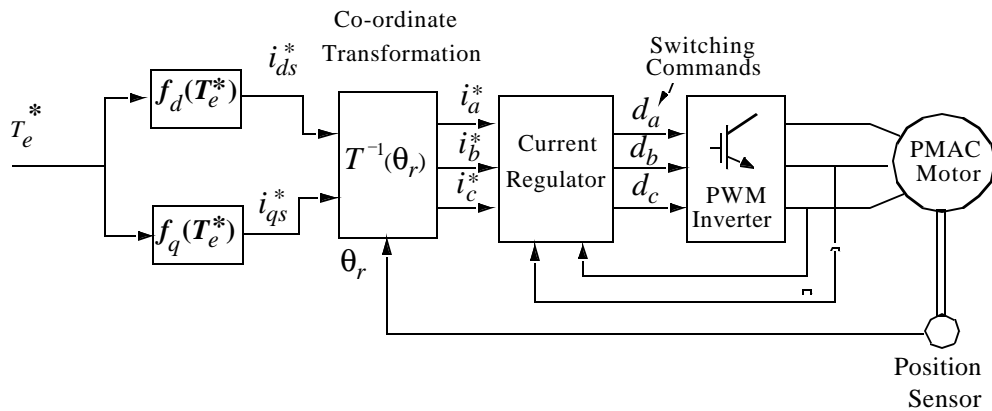


Figure 15.32 Torque control scheme for sinusoidal PMAC motor

The most common means of defining d - q current component commands i_{ds}^* and i_{qs}^* as a function of the torque command T_e^* into is to set a constraint of maximum torque-per-ampere operation which is nearly equivalent to maximizing operating efficiency, see Figure 15.29. Trajectories of the stator current vectors \bar{i}_{qds} the rotor d - q reference frame which obey this maximum torque-per-amp constraint are plotted in Figure 15.33 for a typical salient type of PMAC machine. The trajectories are plotted over a range of torque ampli-

tudes ranging from negative (generating/braking) to positive (motoring) values [35].

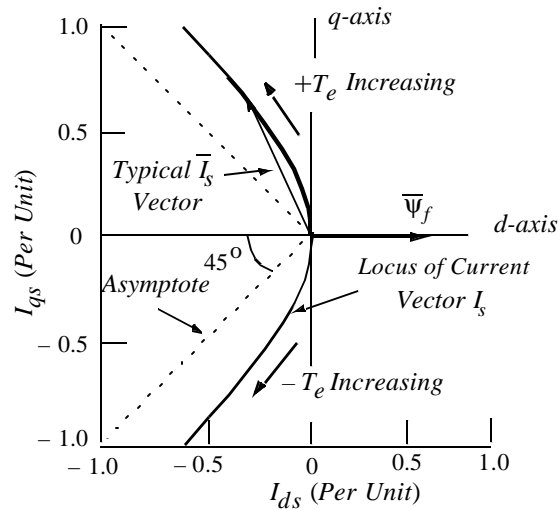


Figure 15.33 Trajectory of stator current vector \bar{I}_s in the synchronous reference frame as torque increases

It can be noted that the maximum torque-per-amp trajectory initially moves along the q -axis for low values of torque before swinging symmetrically into the second and third quadrant towards 45° asymptotes. For motoring operation, this behavior means that maximum torque for a given amount of stator current is developed by advancing the phase angle of the stator phase currents so that they lead their respective back-EMF waveforms by angles between zero and 45° (electrical). The maximum torque-per-amp trajectory reflects the hybrid nature of the PM machine having the capability of producing reluctance torque as well as magnet torque. The corresponding currents I_{ds} and I_{qs} which define the maximum torque per-amp trajectory for the salient pole PMAC machine are plotted in Figure 15.34 [36].

Alternative field-oriented formulations of the sinusoidal PMAC machine control algorithm have been reported that are also capable of achieving high performance by aligning the rotating reference frame with the stator flux phasor rather than with the rotor magnet flux [37],[38]. Although the performance characteristics of these two control formulations are quite similar at low speeds, their differences may become more apparent at higher speeds during the transition from constant torque to constant horsepower operation.

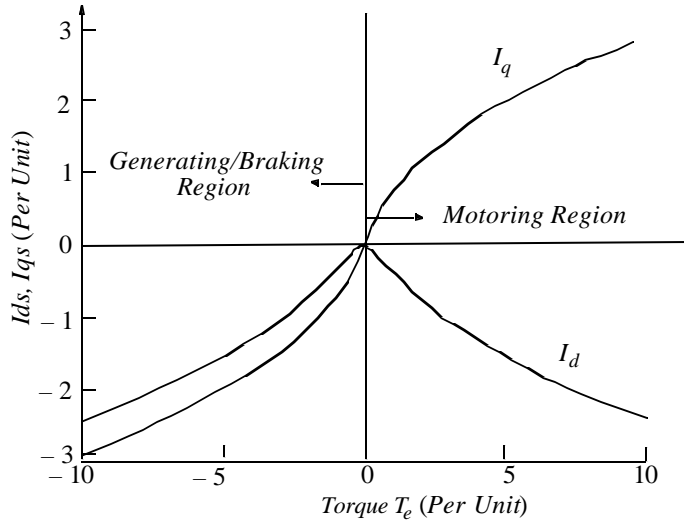


Figure 15.34 Direct and quadrature axis stator currents required to produce maximum torque per ampere for a salient pole permanent magnet machine

15.7.4 Regenerative Braking Operation.

Figure 15.34 shows that the maximum torque-per-amp trajectories are mirror images in the second and third quadrants. Stated in a different way, the I_{qs} function plotted in Figure 15.34 is sensitive to the polarity of the torque command, while the I_{ds} function depends only on its absolute value.

15.7.5 Field Weakening

The load torque limits in the speed range from zero to rated speed is set by the maximum current that can be supplied from the inverter, that is

$$\sqrt{I_{qs}^2 + I_{ds}^2} \leq I_{max} \quad (15.108)$$

The limiting value of Eq. (15.108) can be visualized as a circle in the i_{ds} - i_{qs} plane centered at the origin with radius I_{max} .

Beyond rated speed another constraint is imposed since the inverter pulse width modulator saturates and the output voltage becomes a constant. In this case, clearly

$$\sqrt{V_{qs}^2 + V_{ds}^2} \leq V_{max} = \frac{2}{\pi} V_{bus} \quad (15.109)$$

Using Eqs. (15.104) and (15.105) and rearranging the result, (15.109) can be expressed as

$$\frac{2}{\pi} \frac{V_{bus}}{\omega_e} = i_{qs}^2 + \left(\frac{L_{ds}}{L_{qs}}\right)^2 \left(i_{ds} + \frac{\lambda_m}{L_{ds}}\right)^2 \quad (15.110)$$

Eq. (15.110) can be visualized as a second ellipse in the i_{ds} - i_{qs} plane with a focal point at $i_{qs} = 0$ and $i_{ds} = -\lambda_m/L_{ds}$. The size of the ellipse continues to decrease as the speed ($\omega_r = \omega_e$) increases.

Control of the d - q currents in the field weakening range must be such that the current remains in the circle of Eq. (15.108) and tracks along the shrinking elliptical boundary as shown in Figure 15.35. It can be noted that the d -axis current is driven negative implying a stator MMF component acting to reduce the magnet flux (demagnetize the magnet). When I_{ds} becomes equal to λ_m/L_{ds} , the flux in the magnet has been driven to zero. Further negative increases in I_{ds} must now be prevented. As a result the torque producing component I_{qs} now begins to decrease rapidly and constant horsepower operation can no longer be maintained. The field weakening region in Figure 15.35 corresponds to the segment from point A to point B.

References

- [1] F.M.H. Khater and D.W. Novotny, "An equivalent circuit model for phase back voltage control of AC machines, *IEEE Transactions on Industry Applic.*, vol. 22, no. 5, Sept./Oct., pp. 835-841
- [2] T.A. Lipo, "The analysis of induction motors with voltage control by symmetrically triggered thyristors", *IEEE Trans. on Power Apparatus and Systems*, vol. PAS-90, no. 2, March/April 1971, pp.515-525.
- [3] J. Davoine, R. Perret and H. Le-Huy, "Operation of a self-controlled synchronous motor without a shaft position sensor", in *Conf. Rec. IEEE IAS Annual Meeting*, 1981, pp. 696-701.
- [4] J. Holtz and S. Stadtfeld, "A predictive controller for the stator current vector of ac machines fed from a switched voltage source", in *Conf. Rec. IPEC Conf*, Tokyo, 1983, pp. 1665-1675.

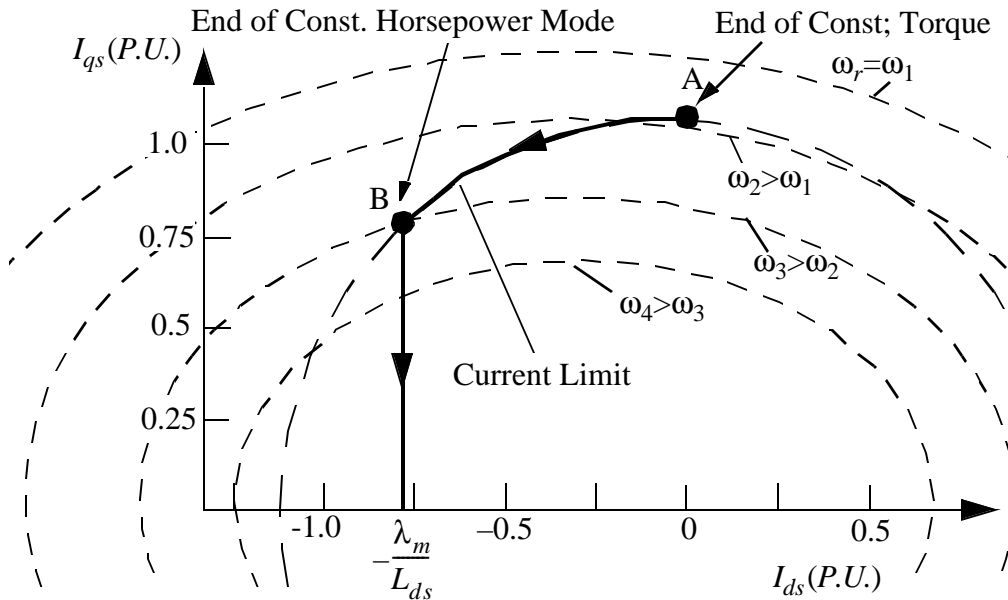


Figure 15.35 Locus of current vector in the d - q plane during operation above rated speed (constant horsepower region is A-B)

- [5] H.W. Van der Broeck, H. Skudelny and G. Stanke, "Analysis and realization of a pulse width modulator based on voltage space vectors", *IEEE Trans. on Industry Applications.*, vol. 24, no. 1, Jan./Feb., 1988, pp. 142-150.
- [6] B. Mokrytzki, "The controlled slip static inverter drive", *IEEE Trans. On Industry and General Applications*, vol. IGA-4, May/June 1968, pp. 312-317.
- [7] K. Koga, R. Ueda and T. Sonoda, "Achievement of high performances for general purpose inverter drive induction motor system", in *Conf. Rec. IEEE IAS Annual Meeting*, 1989, pp. 415-425.
- [8] F. Blaabjerg and J.K. Pedersen, "Ideal PWM-VSI inverter using only one current sensor in the DC-link", in *Conf. Rec. IEE 5th Power Electronics and Variable-Speed Drives Conf.*, 1994, pp. 458-464.
- [9] S.I. Moon and A. Keyhani, "Estimation of induction machine parameters from standstill time-domain data", *IEEE Trans. on Industry Applic.*, vol. 30, no. 6, 1994, pp. 1609-1615

-
- [10] J. Stephan, M. Bodson and J. Chaisson, "Real-time estimation of the parameters and fluxes of induction motors", *IEEE Trans. on Industry Applic.*, vol. 30, no. 3, 1994, pp. 746-758.
- [11] J.A. Capolino, "Identification of induction machine parameters", in *Conf. Rec. of the Int. Aegean Conf. on Electric Machines and Power Electronics*, vol. 2, 1995, pp. 627-637.
- [12] Y. Kishimoto, S. Asaba, K. Nakata and S. Kawatsu, "Control device for induction motor", U.S. Patent 5,231,339, July 27, 1993.
- [13] S.I Moon and A. Keyhani, "Estimation of induction machine parameters from standstill time-domain data", *IEEE Trans. on Industry Applications*, vol. 30, no. 6, 1994, pp. 1609-1615.
- [14] J. Stephan, M. Bodson and J. Chaisson, "Real-time estimation of the parameters and fluxes of induction motors", *IEEE Trans. on Industry Applications*, vol. 30, no. 3, 1994, pp. 746-758.
- [15] J.A. Capolino, "Identification of induction machine parameters", *Proc. of the Int. Aegean Conf. on Electrical Machines and Power Electronics*, vol. 2, 1995, pp. 627-637.
- [16] A. Munoz-Garcia, T.A. Lipo and D.W. Novotny, "A new induction motor open-loop speed control capable of low frequency operation", *IEEE Trans. on Industry Applications*, vol. 34, no. 5, July/August, pp. 813-821.
- [17] D. Leggate and R. Kerkman, "Pulse based time compensator for PWM voltage inverters", in *Conf. Record of IEEE IECON*, 1995, pp. 474-481.
- [18] J.W. Choi, S.I. Yong and S.K. Sul, "Inverter output voltage synthesis using novel dead time compensation", *IEEE Trans. on Industrial Applic.*, vol. 31, no. 5, 1995, pp. 1001-1008.
- [19] Y. Murai, T. Watanabe and H. Iwasaki, "Waveform distortion and correction circuit for PWM inverters with switching lag-times", *IEEE Trans. on Industrial Applic.*, vol. 23, no. 5, 1987, pp. 881-886.
- [20] T. Sukegawa, K. Kamiyama, T. Matsui, and T. Okuyama, "Fully digital, vector controlled PWM-VSI fed AC drives with an inverter dead-time compensation strategy", in *Conf. Rec. IEEE IAS Annual Mtg.*, 1988, pp. 463-469.

-
- [21] J.W. Choi, S.I. Yong and S.K. Sul, "Inverter output voltage synthesis using novel dead time compensation", in *Conf. Rec. IEEE IAS Annual Mtg.*, 1994, pp. 100-106.
- [22] D.W. Novotny and T.A. Lipo, "Vector control and dynamics of AC drives", (book) Oxford Press, Oxford England, 1996.
- [23] R. de Doncker and D.W. Novotny, "The universal field oriented controller", in *Conf. Rec. IEEE IAS Annual Meeting*, Oct. 1988, p. 450-456.
- [24] X. Xu and D.W. Novotny, "Selection of the flux reference for induction machines in the field weakening region", *IEEE Trans. on Industry Applic.*, vol. 28, no. 6, November/December 1992, pp. 1353-1358.
- [25] K.B. Nordin, D.W. Novotny and D.S. Zinger, "The influence of motor parameter deviations in feedforward field orientation drives systems", *IEEE Trans. in Industry Applic.*, vol. IA-21, no. 4, July/August 1985, pp. 1009-1015.
- [26] T. Rowan and R. Kerkman, "A new synchronous current regulator and an analysis of current-regulated PWM inverters", *IEEE Trans. on Industry Applic.*, vol. IA-22, no. 4, July/August 1986, pp. 163-171.
- [27] L. Malesani and P. Tenti, "A novel hysteresis control method for current controlled VSI PWM with constant switching frequency", *IEEE Trans. on Industry Applic.*, vol. IA-26, no. 1, Jan/Feb, 1990, pp. 88-92.
- [28] Q. Yao and D.G. Holmes, "A simple, novel method for variable-hysteresis-band current control of a three phase inverter with constant switching frequency", in *Conf. Rec. IEEE IAS Annual Meeting*, 1993, pp. 1122-1129.
- [29] J. Holtz and S. Stadtfeld, "A predictive controller for the stator current vector of AC machines fed from a switched voltage source", in *Conf. Rec. IPEC*, Tokyo, 1983, pp. 1665-1675.
- [30] A. Nabae, S. Ogasawara and H. Akagi, "A novel control scheme for current-controlled PWM inverters", *IEEE Trans. on Industry Applic.*, vol. 22, no. 4, July/August, 1986, pp. 697-701.
- [31] R. Joetten and G. Maeder, "Control methods for good dynamic performance induction motor drives based on current and voltage as measured quantities", *IEEE Transactions on Industry Applic.*, vol. IA-19, no. 3, May/June 1983, pp. 356-363.

- [32] K. Rajashekara, A. Kawamura and K. Matsuse (editors), “Sensorless control of AC motor drives”, (book) IEEE Press, 1996.
- [33] V.I. Utkin, “Sliding mode control design principles and applications to electric drives”, *IEEE Trans. on Ind. Elec.*, Vol.40, 1993, pp.23-36.
- [34] M. Rodic, K. Jezernik, A. Sabanovic, “Speed sensorless sliding mode torque control of induction motor”, in *Conf. Rec. IEEE-IAS Ann. Meeting*, 2000, pp.1820-1827.
- [35] S. Morimoto, Y. Takeda, T. Hirasaka and K. Taniguchi, “Expansion of operating limits for PM motor by optimum flux weakening”, *IEEE Trans. on Industrial Applic.*, vol. 26, no. 5, Sept.Oct. 1990, pp. 866-871.
- [36] T.M. Jahns, G.B. Kliman and T.W. Neumann, “Interior PM synchronous motors for adjustable-speed drives”, *IEEE Trans. on Industrial Applic.*, vol. 22, no. 4, July/August 1986, pp. 738-747.
- [37] B.K. Bose, “A high-performance inverter-fed drive system of an interior PM synchronous machine”, *IEEE Trans. on Industrial Applic.*, vol. 24, no. 6, Nov./Dec. 1988, pp. 987-998.
- [38] M.A. Bilewski, A. Fratta, L. Giordano, A. Vagati and F. Villata, “Control of high performance interior PM synchronous drives”, in *Conf. Rec. IEEE-IAS Annual Meeting*, 1990, pp. 531-538.